Discrete Signal Processing Techniques for Power Converters

Multi-Carrier Modulation and Efficient Filtering Techniques

by

Jason Forbes

B.Eng., Memorial University of Newfoundland, 2011

A THESIS SUBMITTED IN PARTIAL FULFILLMENT OF
THE REQUIREMENTS FOR THE DEGREE OF

MASTER OF APPLIED SCIENCE

in

The Faculty of Graduate and Postdoctoral Studies

(Electrical and Computer Engineering)

THE UNIVERSITY OF BRITISH COLUMBIA

(Vancouver)

October 2013

Abstract

Digital control has become ubiquitous in the field of power electronics due to the ease of implementation, reusability, and flexibility. Practical engineers have been hesitant to use digital control rather than the more traditional analog control methods due to the unfamiliar theory, relatively complicated implementation and various challenges associated with digital quantization. This thesis presents discrete signal processing theory to solve issues in digitally controlled power converters including reference generation and filtering.

First, this thesis presents advancements made in the field of digital control of dc-ac and ac-dc power converters. First, a multi-carrier PWM strategy is proposed for the accurate and computationally inexpensive generation of sinusoidal signals. This method aims to reduce the cost of implementing a sine-wave generator by reducing both memory and computational requirements. The technique, backed by theoretical and experimental evidence, is simple to implement, and does not rely on any specialized hardware. The method was simulated and experimentally implemented in a voltage-controlled PWM inverter and can be extended to any application involving the digital generation of periodic signals.

The second advancement described in this thesis is the use of simple digital filters to improve the response time of single-phase active rectifiers. Under traditional analog control strategies, the bandwidth of an active rectifier is unduly restricted in order to reduce any unwanted harmonic distortion. This work investigates digital filters as a proposed means to improve the bandwidth, and thereby create a faster, more efficient ac-dc power converter. Finally, a moving average filter is proposed, due to its simple implementation and minor

computational burden, as an efficient means to expand the bandwidth. Since moving average filters are well known and widely understood in industry, this proposed filter is an attractive solution for practicing engineers.

The theory developed in this thesis is verified through simulations and experiments.

Preface

This work is based on research performed at the Electrical and Computer Engineering department of the University of British Columbia by Jason Forbes, under the supervision of Dr. Martin Ordonez. Some experimental validation work was done in collaboration with Matias Anun.

A version of Chapter 2 has been submitted for publication [1].

Versions of Chapter 3 and Chapter 4 have been published at the IEEE Applied Power Electronics Conference and Exposition (APEC) and IEEE Energy Conversion Congress and Exposition (ECCE), respectively [2],[3].

As first author of the above-mentioned publications, the author of this thesis developed the theoretical concepts, performed simulation, and wrote the manuscripts. Advice and technical support was provided from Dr. Martin Ordonez in all three papers. MASc. student Matias Anun developed the experimental platforms and aided in producing and summarizing the experimental captures for papers [2],[3] .

Table of Contents

List of Tables

List of Figures

Acknowledgments

I would like to acknowledge my senior supervisor, Dr. Martin Ordonez, not only for his technical guidance, but also for his support and encouragement throughout the past two years. He helped evolve my technical grasp of the subjects presented within, and reinforced my natural curiosity about the applied sciences, helping me to become a better researcher. For this and more I wish to thank him.

I would also like to thank the other research members of the Alpha Technologies Power Laboratory at the University of British Columbia's Vancouver campus. In particular, I would like to thank Matias Anun, who developed invaluable experimental setups, and Ignacio Galiano Zubrugen, for indulging my occasional need for a sounding board.

Lastly, I would like to acknowledge the National Science and Engineering Research Council for their support and funding.

For my parents

Chapter 1

Introduction

1.1 Motivation

Microprocessors and digital controllers are becoming more common in power converters due to their increased flexibility, robustness, and reproducibility. The proliferation of digitally controlled power converters allows for numerous advancements over a wide range of topics. This work examines two such advancements. First, it examines advancements made to the digital generation of sinusoidal signals used as reference functions in digital pulse-width modulation (PWM). The proposed advancement is named multi-carrier PWM and uses two interleaved carrier frequencies to balance distortion and frequency resolution in reference waveforms without sacrificing computational speed. This is a necessary component for the control of many power-converters relying on a digitally generated periodic reference, including inverters and power factor correctors (PFC). The second contribution made in the area of discrete signal processing is applying the mature field of digital filters to the problem of PFC voltage feedback control. Through this approach, a more efficient, cost-effective PFC can be developed with a fast transient response and low computational overhead. Although often overlooked, simple design and theory are important considerations for the development of power converters for practical applications.

Digital generation of sinusoidal signals is a necessary aspect of modern digital systems. Due to the transcendental nature of the sinusoid, there is no simple formula that can be used to calculate the function $sin(\theta)$ for an arbitrary input θ. Instead, as microprocessors become

more powerful, various techniques (including interpolation and expansive look-up tables) have become the preferred approach for digital sinusoidal synthesis, but the affordability of these systems relies on the existing need for external memory and powerful processors. In low-margin embedded control applications, such as digitally-controlled power converters, computation and memory is at a premium. For sub-dollar microcontrollers, excessive computation time can detract from the efficient control of the converter. Similarly, requiring external memory for an expansive look-up table can unnecessarily increase the cost, size, and overhead of the power converter.

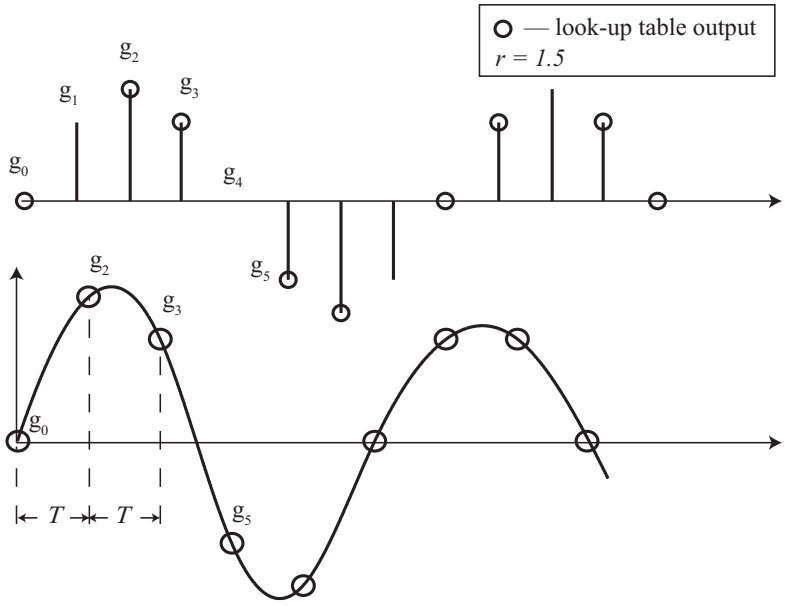

Figure 1.1: Conceptual operation of non-uniformly sampled sinusoidal synthesis. Note the distortion that exists due to the nonuniform quantization error.

Existing sinusoidal synthesis techniques generate sine signals through a look-up table [4]. Using one approach called non-uniform sampling, look-up table based sinusoidal synthesis generates harmonic distortion that is highly dependent on microprocessor word-length [5],[6]. This approach consists of approximating a single period of $sin(\theta)$ with N samples. The N samples correspond to N equidistantly spaced angles, $0 <= \theta_k <= 2\pi$ where $k \in 0, 1, 2, ..., N-1$ (due to symmetry, in practice only $N/4$ points are actually stored in

memory). The approximation occurs due to a non-linear quantization effect seen in Fig. 1.1. A desired angle $\bar{\theta}$ is approximated by the closest stored angle θ_k, such that the fundamental period T_0 is precisely chosen. Operating in this fashion, the digital output of the reference is given by the following equation, where T is the carrier period and r is a coefficient which adjusts the sampling rate, subject to $0 < r \leq \frac{N}{2}$. In the following equations, $< x >_y$ is the modulo operation on x and y, and $round(\cdot)$ is an operation that returns the nearest integer.

$$x[k] = sin\left(\langle round(rk)\rangle_N \frac{2\pi}{NT}\right) \tag{1.1}$$

It can be seen from (1.1) that the fundamental period is given by the following equation.

$$T_0 = \frac{NT}{r} \tag{1.2}$$

Using the notation provided above, the desired angles are determined to be $\bar{\theta_k} = rk\frac{2\pi}{N}$. The angles, which can be approximated to machine precision, are as follows.

$$\Theta = \left\{k\frac{2\pi}{N} \mid 0 < k < N,\ k \in \mathbb{N}\right\} \tag{1.3}$$

For a given angle $\bar{\theta_k}$, the angle quantization error, typically modeled as uniform quantization error, can therefore be defined as:

$$\begin{aligned}\Delta\theta_k &= inf\left\{|\bar{\theta_k} - \phi| \mid \phi + 2\pi n \in \Theta, n \in \mathbb{I}\right\} \\ &= |round(rk) - rk|\ \frac{2\pi}{N}\end{aligned} \tag{1.4}$$

The quantization error of the output signal is complicated by its nonuniform nature.

$$\begin{aligned}\Delta x_k &= 2sin\left(\frac{\Delta\theta_k}{2}\right)cos\left((round(rk)+rk)\frac{\pi}{N}\right)\\ &\approx 2sin\left(\frac{\Delta\theta_k}{2}\right)cos\left(rk\frac{2\pi}{N}\right)\end{aligned} \tag{1.5}$$

Equation (1.5) shows that the output error is dependent on both the angle being generated, and a nonlinear function of the quantization error in that angle. As will be seen, traditional methods of minimizing 1.5 rely on either increasing N or on interpolation. An example of the distortion generated by non-uniformly sampling the look-up table is shown in Fig. 1.1.

The multi-carrier sinusoidal synthesis approach presented in this thesis completely eliminates the sub-harmonics introduced by non-uniform sampling, and reduces the total harmonic distortion (THD). The interleaving of two distinct carrier frequencies as a means of eliminating harmonics is analogous to the current trend of employing distinct dc-sources in multi-level inverters for THD reduction [7], [8].

The second approach, called uniform sampling, also utilizes a look-up table. In this approach, the coefficient r is limited to an integer, such that $\bar{\theta_k} \in \Theta$. When this approach is used, there is no quantization error in the output apart from machine precision, since $round(rk) = rk$ for $r, k \in \mathbb{I}$. This approach is visualized in Fig. 1.2. While effective in eliminating the quantization error described in (1.5), uniformly-sampled sinusoidal generation unnecessarily limits the set of frequencies that can be synthesized, as will be shown in Chapter 3. Both methods described above rely on the accuracy of the assumption that the carrier frequency T is fixed. This work is motivated by the need for an efficient, computationally inexpensive method for sinusoidal synthesis that balances quantization error and memory size without limiting the set of achievable frequencies.

One of the many applications for sinusoidal synthesis is for reference generation in pulse-

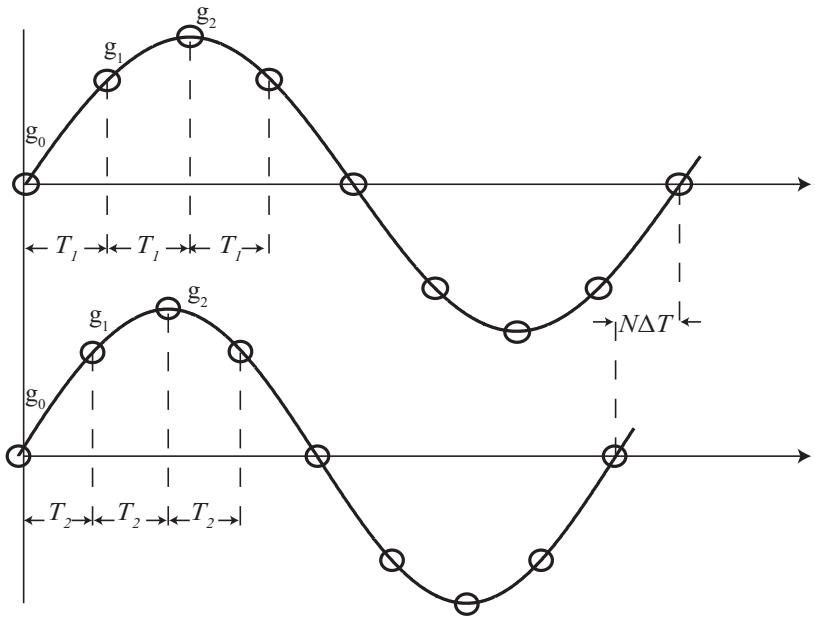

Figure 1.2: Uniformly sampled sinusoidal synthesis exhibiting frequency resolution.

width modulated (PWM) controlled power converters. An inexpensive approach to eliminating subharmonic distortion and decreasing THD in digital reference generation will allow for more efficient power converters, implemented using low-cost hardware. This work will specifically study carrier-based single-phase inverters as an application for the sinusoidal synthesis techniques discussed within.

The second contribution to digital signal processing for power converters in this thesis is the elimination of harmonic content from the control loop of active rectifiers, also known as power factor correctors (PFC). A PFC is an ac-dc converter that aims to match the input voltage and current in both shape and phase [9]. The circuit diagram of a PFC with traditional feedback loops is shown in Fig. 1.3. The input voltage for the PFC is a sinusoidal signal, typically at line frequency. The PFC attempts to emulate a resistive load by shaping the inductor current i_L to match the input voltage $|v_i|$. To accomplish this, a variety of different current controllers are used [9]-[11]. The inner control loop compares the inductor current to a current reference to determine the switching pattern necessary to achieve the

correct waveform. An outer control loop is needed to set the control voltage $\hat{v}_{control}$, which controls the dc output voltage.

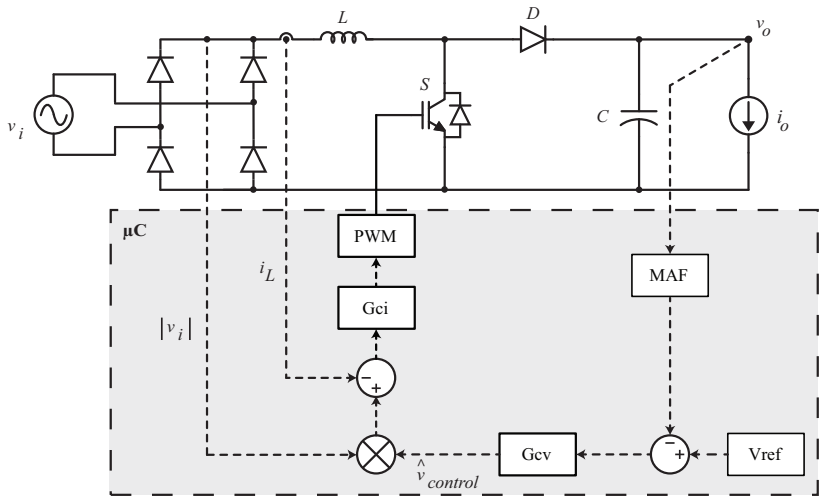

Figure 1.3: Circuit diagram of a PFC boost converter with a voltage feed-forward current loop and placement of MAF filter in the voltage feedback loop.

Typically, to facilitate the rectification of a sinusoidal inductor current, the output capacitor voltage will need to exhibit a low frequency ripple, the size of which is determined by the size of the capacitor [12]. If the spectrum of the bus voltage is examined, it will be found to contain components at the ripple frequency (which is twice the line frequency) and its harmonics. The reason for which will be examined as part of the literature review. When these components are fed back through the current controller, they can cause an unwanted increase in inductor current THD. Ideally, the signal of the bus voltage will contain no ripple or harmonics that influence the current control loop.

The traditional method of reducing the harmonic content relies on techniques developed for analog systems, the most common of which is a PI controller. The PI controller and plant act as a low-pass filter, which reduces ac content in the output signal such that the inductor current THD is minimized. This action unduly restricts the bandwidth, and therefore the transient response, of the PFC, as can be seen in Fig. 1.4.

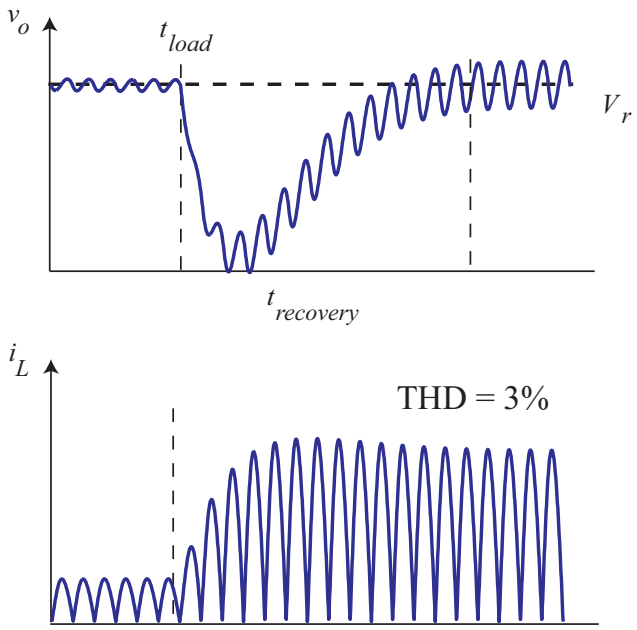

Figure 1.4: Without MAF in the feedback loop, output voltage experiences a recovery time of seven line cycles and inductor current has a THD of 3%.

1.2 Literature Review

1.2.1 Digital Sinusoidal Synthesis

From (1.1), it is readily seen that for an integer r, the function $f[n]$ returns a uniformly sampled sine wave but, as will be shown, this constraint can limit the period resolution. It has been shown that for non-integer r, there is adequate resolution. For an r represented by an unsigned integer of size n-bits, the frequency resolution $\Delta f_0 = \frac{1}{T2^{-n}}$, where T is the carrier period. Using a $16-bit$ application, this resolution is adequate for many applications [13].

Using this method, the resulting non-uniformly sampled function introduces distortion. It has been shown that, generally, the THD introduced by this method is dependent on the value of r. More specifically, the distortion depends upon the M where $M = inf\{M|Mr \in \mathbb{N}, M \in \mathbb{N}\}$ [14]. Furthermore, in the case of sinusoidal oscillators, the maximum and minimum THD is

given by $M \to \infty$ and $M = 2$, respectively. The fundamental power of the generated signal using non-uniform sampling varies with the table size N, and is provided by the following equation, assuming that the total power is $P_{tot} = 1$ and $M \to \infty$ [15].

$$P_1 = \frac{sin^2(\pi/N)}{\pi/N} \tag{1.6}$$

It has also been shown that under certain conditions, the reference waveform can exhibit sub-harmonic distortion. The condition for this is provided by the following equation [16].

$$N < 2Mr \tag{1.7}$$

It can be seen from (1.6) that P_1 is maximized as $N \to \infty$. In practice, N corresponds to the number of samples stored in a digital look-up table, and is therefore limited by the amount of available memory. Furthermore, as the sine function is expected to be called often, it is worthwhile to have the look-up table stored "on-chip" to avoid lengthy fetch operations from external memory. On-chip memory is limited for all but high-end DSPs. As an alternative, external memory is available, and commonly used in low-end microcontrollers, but this has an associated cost that can be detrimental in low-margin industries.

To circumvent the need for an excessively large look-up table, an alternative method, and one that is used in practice, is to interpolate between look-up table entries in order to reduce error in non-integer sample rates. One of the most common techniques, and one that is often used in practice, is Taylor expansion around the desired point $sin(\bar{\theta})$ where h is the difference between the desired angle $\bar{\theta}$ and the nearest stored angle θ_k [17].

$$sin(\bar{\theta}) = sin(\theta_k) + h\, cos(\theta_k) + O(h^2) \tag{1.8}$$

If N, the length of the look-up table, is a multiple of four, a phase shift of $\pi/2$ corresponds

exactly to a $N/4$ samples such that $cos(\theta_k) = sin(\theta_{k+N/4})$, (1.8) can be rewritten as follows.

$$sin(\bar{\theta}) = sin(\theta_k) + h\ sin(\theta_{k+N/4}) + O(h^2) \tag{1.9}$$

This form of interpolation relies on two fetch operation, one multiplication, and one addition; moreover, it carries the computational burden required in determining h and the nearest stored value θ_k. In modern microcontroller libraries, a call to a similar interpolating look-up table takes 40 clock-cycles [18]. The multiplication has been found to be a significant contributor to increased computational burden, and should be avoided [17].

Another interpolation technique uses a polynomial interpolation by approximating a sine function by an 8^{th} order polynomial. This interpolation method relies on specific hardware for efficient calculation, or on the use of many multipliers to perform the squaring operations. The technique exhibits low THD, but at the cost of increased computational burden [19].

Quasi-linear interpolation improves upon the previous method by using a combination of linear and parabolic polynomial interpolation techniques to generate a sine wave. This interpolation provides modest gains, as the piece-wise quadratic combination is better suited to modern parallelized and pipe-lined computer architectures. This algorithm is implemented in a specialized FPGA to take full advantage of the parallelization available. Microcontroller and DSP implementations where hardware flexibility is not available limit the efficiency of this approach [20].

1.2.2 Voltage Source Inverters

PWM inverter systems are characterized by a high-frequency constant-amplitude pulse train (carrier). PWM is usually achieved by making a direct comparison, termed natural modulation, between the amplitudes of a modulating wave and a carrier wave. We cannot analyze PWM using a traditional Fourier series, since the PWM waveform is not guaranteed to be

periodic. Even if it is periodic, results will not be accurate, as sideband and base-band frequencies will coincide. Instead a double-Fourier analysis is needed. Any fixed modulating process can be modeled using a 3-dimensional model, such that the modulating waveform is represented as an infinitely large number of parallel contours in a 2-dimensional plane. The height of these contours, represented in a third dimension, correspond to the PWM output. The intersection between the contour plane and the carrier trajectory $y = \frac{T}{T_0}x$ is projected to produce the PWM waveform, where T is the carrier period and T_0 is the fundamental period. The periodicity in both carrier and fundamental leads to the formulation of the double Fourier series [21].

This analysis is a useful tool for describing naturally-sampled PWM, and provides insight on how the harmonic spectrum of the modulated waveform is dependent on the harmonic structure of the reference. However, this method is unable to describe the harmonic effects that occur in digital systems where, in contrast with regular sampling, the modulating waveform is discretized and the pulse durations are determined by discrete modulation values. Regular sampling enables pulse configuration to be unambiguously defined, allowing for optimum pulse positioning for the cancellation of particular harmonics, but it is dependent on uniform sampling times [22].

Using these analysis tools, many control schemes and performance criteria have been developed. The first performance criteria considered is the distortion factor, which is the root-mean-square (RMS) distortion current for a given scheme normalized against the RMS distortion current based on a six-step inverter, which removes the influence of the machine dependent inductance. The next performance criterion is the harmonic spectra, which can be calculated using the analysis tools mentioned above, and from which the THD can be calculated. This is the analysis criterion of choice. Other criteria include torque ripple, switching frequency, and control-loop bandwidth [24]. The THD equation that will be used as the primary criterion for analysis is presented below, where P_i is the power of the i^{th}

harmonic.

$$THD = \frac{\sqrt{\sum_{i=2}^{\infty} P_i^2}}{P_1} \tag{1.10}$$

Improving the harmonic content of carrier-based PWM converters is important as low-harmonic and sub-harmonic interference can affect performance in applications such as grid-connected PV inverters [25]. Multi-carrier PWM is one in a series of novel PWM techniques developed recently to achieve lower THD in inverters, including carrier phase shifting in parallel-connected inverters [26], carrier phase-shifting in cascaded inverters [27], level-shifting in multi-level inverters [28], and decomposing the reference in multiple dimensions for two-level converters [29]. Recent work has shown that there is still significant reductions to be made in THD through modulation strategies based on non-uniform sampling. One method implements a nonuniform sampling function that can be reconstructed using a dual wavelet function [30], [31].

1.2.3 PFC Control

As described above, the dc-voltage output will contain a ripple twice the frequency of the input sinusoidal signal. This is further complicated by the existence of higher-order harmonics in the input signal due to rectification; these harmonics will also exist in the output voltage for single-phase PFCs [32]. The time domain output of a single-phase PFC with a ripple and harmonics is shown in Fig. 1.5(a). As can be seen in the frequency domain, shown in Fig.1.5(b), this ripple is comprised of frequency components at twice the line frequency and its harmonics. The feedback of this harmonic content will create an unwanted distortion in the PWM control signal.

There are many control techniques for the current-shaping in PFCs. Three-phase systems can take advantage of space-vector and dead-beat control strategies [33]. Other methods use

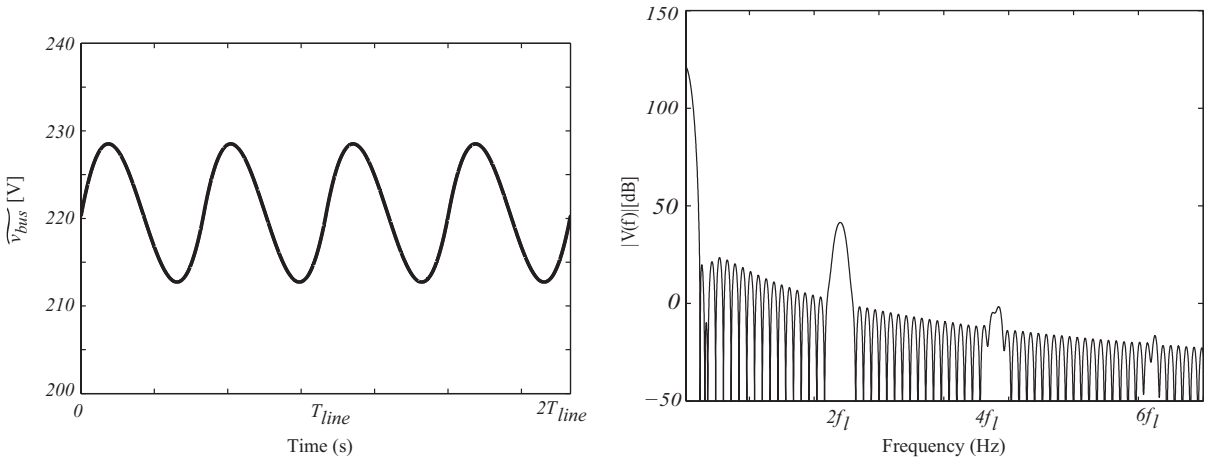

(a) (b)

Figure 1.5: (a) Time-domain output of a single-phase PFC exhibiting a ripple with fundamental frequency of twice the line frequency. (b) Harmonic spectrum of a PFC dc-output with inverter-generated input signal, visualized using a $600pt$ Hamming window.

a zero-cross detector coupled with an input-current estimator to determine the PFC switching pattern [34] and other predictive control methods [35],[36]. The current-controller chosen in this work is the popular average-current control, seen in Fig. 1.3 [9]. In this control scheme, the dc output-voltage of the single-phase PFC is used to scale the input voltage, the result of which is used as a reference for the current-controller. If there is any harmonic content in the dc output-voltage, the current reference will be distorted, and therefore the inductor current will exhibit distortion.

Using small signal analysis, the voltage loop of a PFC can be modeled as a simplified single pole [9]. With a PI controller, the voltage loop of a PFC can be controlled to produce an arbitrary large bandwidth, only limited by the sample rate. But with such a large bandwidth, the ripple and harmonics in the output voltage will become amplified and greatly distort the inductor current. To reduce this, the PI compensation is adjusted to produce an attenuating effect for signals at and above the ripple frequency. It has been shown that to provide adequate attenuation, the system bandwidth is greatly reduced, often to values less than $1Hz$ [10]. With such a low bandwidth, the traditionally-compensated PFC is unable to

quickly respond to transients.

Previous digital filters have been proposed to overcome this bandwidth limitations by using discrete algorithms. A two-pole, two-zero digital notch filter has been proposed and implemented as a simple means to remove the ripple from the voltage feedback loop. This digital notch filter is capable of filtering out the ripple frequency, but the harmonics remain [37]. The transfer function for the digital notch filter is given by the following equation, where f_0 is the filter frequency, f_s is the sample frequency, and r is a parameter between $0 < r < 1$ which determines the steepness of the filter roll-off. This filter has the advantage of removing the ripple frequency and requires a minimum memory storage to do so.

$$H_z = \frac{1 - 2\,cos(2\pi f_o/f_s)z^{-1} + z^{-2}}{1 - 2r\,cos(2\pi f_o/f_s))z^{-1} + r^2 z^{-2}} \tag{1.11}$$

It has been shown that the computation time needed for this filter can increase the control loop by $12\mu s$. In inexpensive micro-controllers, there is also a limitation in the precision of the roll-off factor r. In previously conducted experiments, the steepest roll-off factor that could be used without causing filter instability was $r = 0.95$ [38].

A modified comb filter has also been presented. The comb filter is designed to notch a frequency and its harmonics while returning to a unitary gain between notches, maximizing the bandwidth's potential [39], [40]. The transfer function for a comb filter is given by the following equation, where M is the kernel size of the filter and r is a parameter between $0 < r < 1$ that determine the steepness of the filter roll-off.

$$H_z = \frac{1 - z^{-(M+1)}}{1 - z^{-1}} \frac{1 - rz^{-1}}{1 - r^{M+1} z^{-(M+1)}} \tag{1.12}$$

To filter a specific frequency, f_0, the kernel size M and sample frequency f_s must be chosen such that $f_o = f_s/(M + 1)$. From analyzing the transfer function (1.12), it can be seen that the comb filter requires $2M$ samples to be recorded in memory, M input samples

and M output samples, for the algorithm to be computed efficiently in real-time. Similarly to the notch filter, there is a limitation in the roll-off factor r, such that values $r \to 1$ increase the chance of instability due to quantization effects.

1.3 Organization

This thesis is organized as follows.

Chapter 2 introduces the multi-carrier method as a means of decreasing harmonic distortion in sinusoidal reference waveforms. This chapter derives the associated harmonic spectrum of a sinusoidal signal synthesized through such a method, after which the THD can be compared to non-uniformly sampled sinusoidal generation. A proof is supplied which determines the sufficient conditions necessary to eliminate half of the offending harmonics and further reduce the THD. It is shown that multi-carrier PWM outperforms non-uniform reference generation in terms of THD and memory minimization.

In Chapter 3, the synchronization capability for ac-dc/dc-ac power converters is considered. Under digital PWM, the number of fundamental frequencies that can be achieved is limited due to quantization phenomenon inherent in digital systems. This is analyzed for uniformly sampled and multi-carrier sinusoidal generation. It is shown that multi-carrier PWM significantly outperforms uniformly sampled reference generation in terms of synchronization capabilities. Implementation details for multi-carrier PWM in inverters are considered, and experimental and simulation validations of the theory are presented.

Chapter 4 introduces the moving average filter (MAF) as a practical and efficient digital filtering technology to eliminate the harmonic content in closed-loop operation of ac-dc/dc-ac converters. This filter is necessary to improve the sluggish behavior of traditionally controlled ac-dc/dc-ac converters without increasing the THD. A theoretical derivation of the filter is presented, comparing it to other common digital filtering techniques with an emphasis on

minimizing computation and memory requirements. Lastly, experimental and simulation results confirm the significant improvement in response time over PI controllers in the case of the PFC.

Lastly, Chapter 5 presents a summary of the work completed within the thesis as well as concluding remarks.

Chapter 2

Derivation and Analysis of Multi-Carrier PWM

2.1 Harmonic Spectrum of Multi-Carrier Digital Synthesis

This chapter introduces a method of decreasing the quantization error and memory requirements of the sine-waveform reference, while maintaining low computational burden. This is accomplished by interleaving two carrier frequencies, a unique technique that is ideal for PWM-based sinusoidal synthesis such as those in inverters. Each output period is composed of PWM pulses generated at two distinct carrier frequencies in order to generate a single coherent output waveform. Fig. 2.1 compares the advantages of the proposed method to the standard method. Advantages include the reduction in memory size for equal THD and the complete elimination of sub-harmonic distortion.

To evaluate the THD of the resulting signal, the frequency spectrum $Y(\omega)$ is determined in terms of the uniformly sampled signal $g^a(t)$, with frequency spectrum $G^a(\omega)$. The following discussion relates to the THD of the reference waveform before it is modulated by PWM, and does not include the harmonic distortion introduced by this modulation, as conventional techniques do not allow for variable carrier frequencies.

A sequence of the samples $y(t)$ is defined and acts as the reference for pulse width mod-

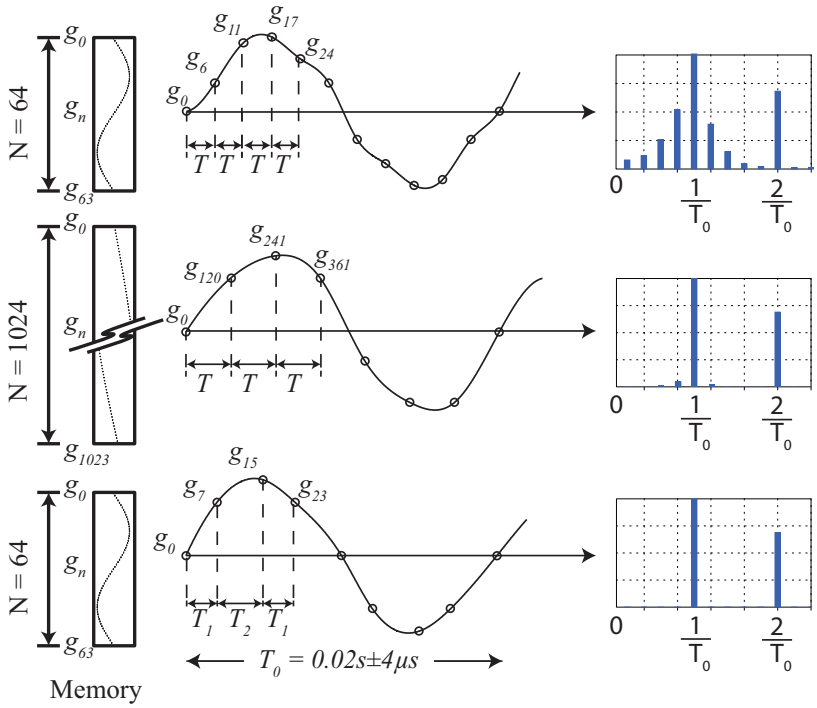

Figure 2.1: Reference generation procedure for digital PWM using traditional look-up table of sizes $N = 64$ (top) and $N = 1024$ (middle) compared with the proposed multi-carrier method (bottom). The proposed method uses less memory, eliminates sub-harmonic oscillations, and achieves less THD. In this figure, the time-domain distortion is exaggerated for emphasis.

ulation. An example of this is shown in Fig. 2.2.

$$y(t) = \sum_{n=-\infty}^{\infty} g(t)\delta\left(t - t_n\right) \tag{2.1}$$

A further constraint is imposed such that only two carriers, with periods T_1 and T_2, are used.

$$t_{n+1} - t_n \in \{T_1, T_2\} \tag{2.2}$$

The sequence $y(t)$ defined in (2.1) is periodic with period $T_0 = NT$, where T is defined as the effective carrier and $N \in \mathbb{N}$ is the number of samples in the period. It is clear from

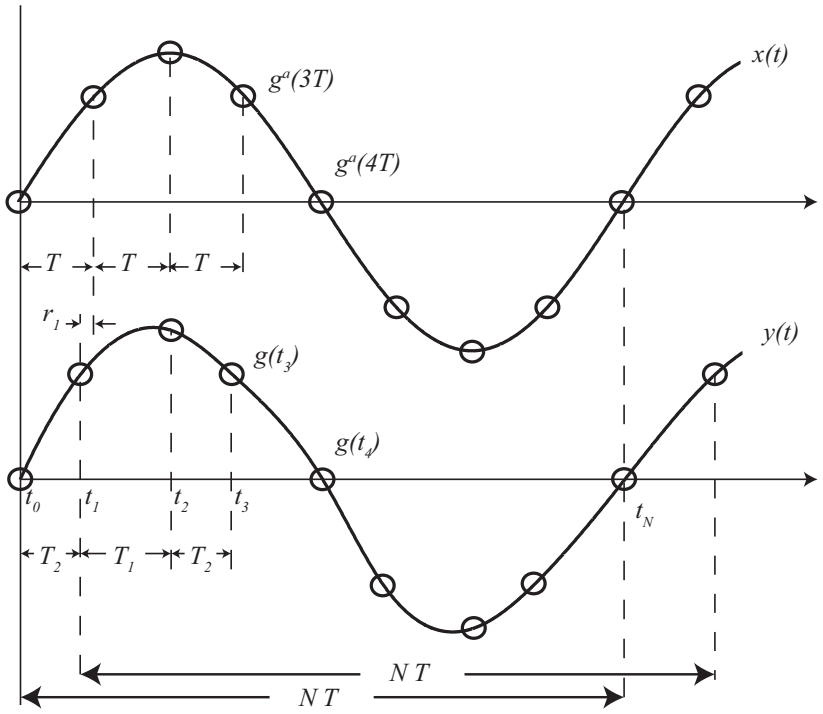

Figure 2.2: Reference generated by outputting $N = 8$ samples using multi-carrier sinusoidal synthesis (top). The samples, stored in a look-up table, are generated by uniformly sampling an ideal waveform (bottom).

this representation that the following is true.

$$g(t_n) = g(t_{n+N}) \tag{2.3}$$

The sequence $y(t)$ can be generated by transforming the uniformly sampled signal $g^a(t)$, which is also periodic in NT, as follows. Let $x(t)$ be the signal $g^a(t)$ sampled with a sampling period T.

$$x(t) = \sum_{n=-\infty}^{\infty} g^a(t)\delta\left(t - nT\right) \tag{2.4}$$

The sequence $x(t)$ can be divided into N sub sequences as follows.

$$
\begin{aligned}
x_0(t) &= \sum_{n=-\infty}^{\infty} g^a(t)\delta\left(t - nNT\right) \\
x_1(t) &= \sum_{n=-\infty}^{\infty} g^a(t+T)\delta\left(t - nNT\right) \\
&\vdots \\
x_m(t) &= \sum_{n=-\infty}^{\infty} g^a(t+mT)\delta\left(t - nNT\right) \\
&\vdots \\
x_{N-1}(t) &= \sum_{n=-\infty}^{\infty} g^a(t+(N-1)T)\delta\left(t - nNT\right)
\end{aligned} \tag{2.5}
$$

The Fourier transform of the m$^{\text{th}}$ sub-sequence can be found by applying common transformations [41].

$$
X_m(\omega) = \frac{1}{NT}\sum_{k=-\infty}^{\infty} G^a\left(\omega - k\frac{2\pi}{NT}\right) e^{j(\omega - k\frac{2\pi}{NT})mT} \tag{2.6}
$$

The original sequence (2.1) can now be reconstructed by delaying each sub-sequence $x_m(t)$ by t_m.

$$
y(t) = \sum_{m=0}^{N-1} x_m(t - t_m) \tag{2.7}
$$

Due to the linearity of (2.7), its Fourier transform is easily found.

$$
Y(\omega) = \sum_{m=0}^{N-1} X_m(\omega)e^{-j\omega t_m} \tag{2.8}
$$

In (2.8), $Y(\omega)$ is the Fourier transform of the original sequence $y(t)$; $X_m(\omega)$ is the Fourier transform of sequence $x_m(t)$, and $G^a(\omega)$ is the Fourier transform of the uniformly sampled

signal which, when outputted at non-uniform times $t_0, t_1, ...$, generates the sequence $y(t)$.

Next, we define a term r_m which is the phase error $mT - t_m$. Let us also assume that the term $G^a(\omega) = 2\pi\delta(\omega - \omega_0)$, as this will aid us in defining the THD of the inverter. Introducing these terms into (2.6), a simplified expression can be developed.

$$Y(\omega) = \frac{2\pi}{T} \sum_{k=-\infty}^{\infty} A[k]\delta\left(\omega - \omega_0 - k\frac{2\pi}{NT}\right) \tag{2.9}$$

$$A[k] = \frac{1}{N} \sum_{m=0}^{N-1} e^{j\omega_0 r_m} e^{jk(r_m - mT)\frac{2\pi}{NT}} \tag{2.10}$$

To determine the THD of this harmonic spectrum, first we must determine the phase error r_m. Its definition is repeated for clarity below.

$$r_m = mT - t_m \tag{2.11}$$

Using (2.2) and the fact that one period has a length NT, we can define an integer λ subject to the constraint $0 \leq \lambda \leq N$ to define the period length as follows.

$$NT = \lambda T_1 + (N - \lambda)T_2 \tag{2.12}$$

For the m$^{\text{th}}$ sample, the time t_m can be determined in a similar fashion by introducing an integer ϕ_m subject to the constraints $0 \leq \phi_m \leq m$ and $\phi_{N-1} = \lambda$.

$$t_m = \phi_m T_1 + (m - \phi_m)T_2 \tag{2.13}$$

Combining (2.11), (2.12), and (2.13), the phase error can be defined in terms of λ and ϕ_m, the number of samples outputted with carrier T_1 over NT and t_m, respectively. We also define ΔT as the difference between the two carrier periods $\Delta T = T_1 - T_2$.

$$r_m = \left(m\frac{\lambda}{N} - \phi_m \right) \Delta T \tag{2.14}$$

To ensure the THD of the resulting output is as low as possible, the phase error is minimized with respect to ϕ_m. How this is implemented in practice will be the subject of Chapter 3. Assuming the previously defined constraints on ϕ_m are enforced, the following relationship is found.

$$\phi_m = \left\lceil m\frac{\lambda}{N} \right\rceil \tag{2.15}$$

Substituting (2.15) into (2.14), the following relationship is found.

$$\begin{aligned} r_m &= m\tfrac{\lambda}{N} - \left\lceil m\tfrac{\lambda}{N} \right\rceil \\ &= \tfrac{\Delta T}{N} \left\langle m\lambda - 1 \right\rangle_N \end{aligned} \tag{2.16}$$

Using a microprocessor, the smallest difference between two carriers, ΔT, is the clock period. For effective PWM operation, it has been proposed in [6] that 8-bits of PWM resolution is sufficient, or $\Delta T/T < 0.004$. From (2.16), it can be seen that $r_m \leq \Delta T$ for all $m \in \mathbb{N}$. It follows that $r_m \leq \Delta T << T$. Therefore, under typical PWM operation, it is a reasonable assumption that $r_m - mT \approx -mT$ for all $m \in \mathbb{N}$. Using this assumption and (2.16), the spectrum coefficients $A(k)$ for $G^a(\omega) = 2\pi\delta(\omega - \omega_0)$ can represented by the following equation.

$$A[k] \approx \frac{1}{N} \sum_{m=0}^{N-1} e^{j2\pi \frac{\Delta T}{N^2 T} \langle m\lambda - 1 \rangle_N} e^{-jkm\frac{2\pi}{N}} \tag{2.17}$$

From the frequency spectrum given in (2.9), it can be seen that the coefficients $A[k]$ defined in (2.17) determine the amplitude of the frequency components.

For a sinusoidal reference, such as that used with an inverter, the frequency spectrum of

the uniformly-sampled sine wave is $G^a(\omega) = j\pi(\delta(\omega+\omega_0) - \delta(\omega-\omega_0))$. Using the theory provided above, the resulting spectrum is determined to be as follows.

$$\begin{aligned} Y(\omega) =& \frac{j\pi}{T}\left(\sum_{k=-\infty}^{\infty} A_+[k]\delta\left(\omega+\omega_0-k\frac{2\pi}{NT}\right) - \right. \\ & \left. \sum_{k=-\infty}^{\infty} A_-[k]\delta\left(\omega-\omega_0-k\frac{2\pi}{NT}\right)\right) \\ A_+[k] \approx& \frac{1}{N}\sum_{m=0}^{N-1} e^{-j2\pi\frac{\Delta T}{N^2T}\langle m\lambda-1\rangle_N} e^{-jkm\frac{2\pi}{N}} \\ A_-[k] \approx& \frac{1}{N}\sum_{m=0}^{N-1} e^{j2\pi\frac{\Delta T}{N^2T}\langle m\lambda-1\rangle_N} e^{-jkm\frac{2\pi}{N}} \end{aligned} \tag{2.18}$$

Employing a change of variables in the summation index and considering that $A_+[k] = A_-^*[N-k]$, a simplified expression can be found in terms of the previously defined coefficients (2.17).

$$\begin{aligned} Y(\omega) =& \frac{2\pi}{T}\sum_{k=-\infty}^{\infty} B[k]\delta\left(\omega-\omega_0-k\frac{2\pi}{NT}\right) \\ B[k] =& \frac{j}{2}(A^*[N-k-2] - A[k]) \end{aligned} \tag{2.19}$$

The harmonic spectrum for the proposed method is presented in Fig 2.3. The relative size of the harmonics are shown in different scales to better show the harmonic structure.

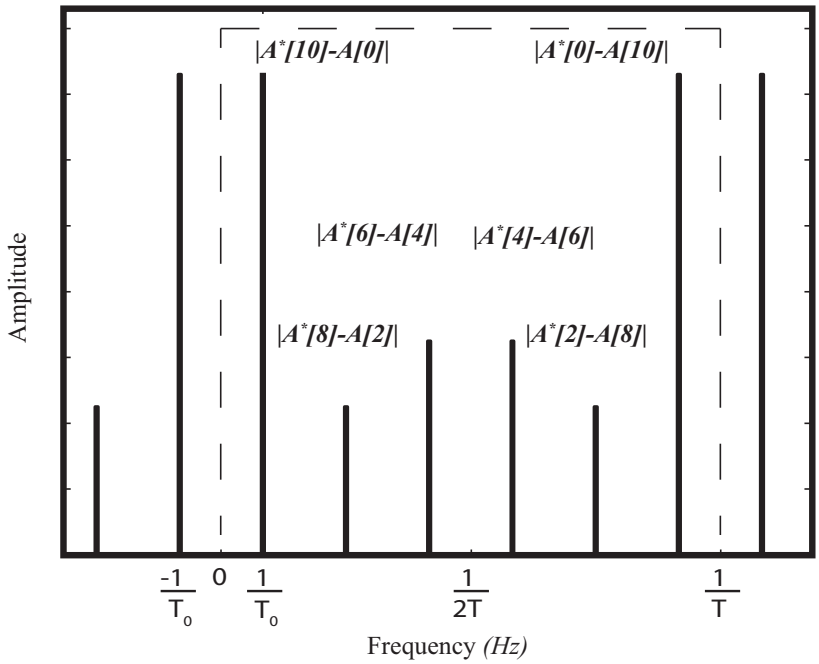

Figure 2.3: The frequency spectrum of a multi-carrier sinusoidal reference generated from a table of $N = 12$ points. The spectrum is periodic, with period $1/THz$.

2.2 Harmonic Distortion of Multi-Carrier Based Sinusoidal Reference

The first obvious benefit of this method is that it can be designed such that the coefficients $B[k] = 0$ for odd k. Sufficient conditions for this to be true are that both N and λ are even. The proof for this is as follows. For conciseness, we will introduce the constant $\beta = 2\pi\frac{\Delta T}{N^2T}$ and the notation $< x >_y$ to denote $x \, mod \, y$.

$$
\begin{aligned}
0 =& \frac{j}{2}(A^*[N-k-2] - A[k]) \\
=& \frac{-j}{2N}\sum_{m=0}^{N-1} e^{-j\frac{2\pi}{N}km}\left(e^{j\beta\langle m\lambda-1\rangle_N)}e^{j\frac{2\pi}{N}m} - \right. \\
& \left. e^{-j\beta\langle m\lambda-1\rangle_N}e^{-j\frac{2\pi}{N}m}\right)e^{-j\frac{2\pi}{N}m} \\
=& \frac{1}{N}\sum_{m=0}^{N-1} e^{-j\frac{2\pi}{N}m(k+1)} sin\left(\beta\left\langle m\lambda-1\right\rangle_N + \frac{2\pi}{N}m\right)
\end{aligned} \tag{2.20}
$$

Given that k is odd, $k+1$ must be even; therefore we can replace it with index $2l$. We will also use the fact that N is even to split the summation.

$$
\begin{aligned}
& \sum_{m=0}^{N/2-1} e^{-j\frac{2\pi}{N}2ml} sin\left(\beta\left\langle m\lambda-1\right\rangle_N + \frac{2\pi}{N}m\right) \\
=& -\sum_{m=N/2}^{N-1} e^{-j\frac{2\pi}{N}2ml} sin\left(\beta\left\langle m\lambda-1\right\rangle_N + \frac{2\pi}{N}m\right) \\
=& -\sum_{m=0}^{N/2-1} e^{-j\frac{2\pi}{N}2\left(m+\frac{N}{2}\right)l} sin\left(\beta\left\langle\left(m+\frac{N}{2}\right)\lambda-1\right\rangle_N \right. \\
& \left. + \frac{2\pi}{N}\left(m+\frac{N}{2}\right)\right) \\
=& \sum_{m=0}^{N/2-1} e^{-j\frac{2\pi}{N}2ml} sin\left(\beta\left\langle\left(m+\frac{N}{2}\right)\lambda-1\right\rangle_N + \frac{2\pi}{N}m\right)
\end{aligned} \tag{2.21}
$$

One case where this equality is always true is when the m^{th} summation terms are equal. A sufficient condition for this to be true is if the arguments of both the sine functions are equal.

$$\begin{aligned}
&\beta \langle m\lambda - 1\rangle_N + \frac{2\pi}{N}m = \beta \left\langle \left(m + \frac{N}{2}\right)\lambda - 1 \right\rangle_N + \frac{2\pi}{N}m \\
&\langle m\lambda - 1\rangle_N = \left\langle \left(m + \frac{N}{2}\right)\lambda - 1 \right\rangle_N \\
&\left\langle -\frac{N}{2}\lambda \right\rangle_N = 0 \\
&\therefore \lambda \; is \; even
\end{aligned} \tag{2.22}$$

This proves the former claim that $B[k] = 0$ for odd k under the conditions that N and λ are even. This has one profound consequence; unlike other methods proposed [16],[15], there is no possibility of subharmonic components using the multi-carrier method proposed in this thesis.

From the frequency spectrum representation of the multi-carrier based sinusoidal reference given in (2.19), it can be seen that the coefficients $B(k)$ determine the amplitude of the frequency components. Analyzing (2.17), we see that the coefficients $A(k)$, and therefore $B(k)$, are periodic on k with period N. This leads to the frequency spectrum $Y(\omega)$ being periodic on ω with period $2\pi/T \; rads$. It should also be noted that using the sampling theorem, the unsampled signal can be reconstructed by including only harmonics of frequency $|f| \leq \frac{1}{2T}$ [41]. Using this knowledge, the normalized total power of the reference sinusoid can be calculated as follows.

$$P_{total} = \sum_{k=0}^{N/2-1} |B[k]|^2 \tag{2.23}$$

Therefore, the THD of a multi-carrier generated sinusoidal reference can be calculated through the following equation.

$$THD = \frac{\sum_{k=0}^{N/2-1} |B[k]|^2 - |B[0]|^2}{|B[0]|^2} \tag{2.24}$$

Equations (1.6) and (2.24) were used to compare the THD of the traditional non-uniform sampling digital synthesis of a sinusoidal reference with that of the proposed method; the results of this comparison are featured in Fig. 2.4. These results are based on the assumption made in (2.17) and are valid only for $\Delta T \ll T$. Due to the limits of digital PWM, in practice $\Delta T/T < 0.01$, in which case the reference generated with multi-carrier PWM has a THD that is several orders of magnitude less than that produced using traditional non-uniform sampling. If ΔT is minimized, it is equivalent to the PWM clock.

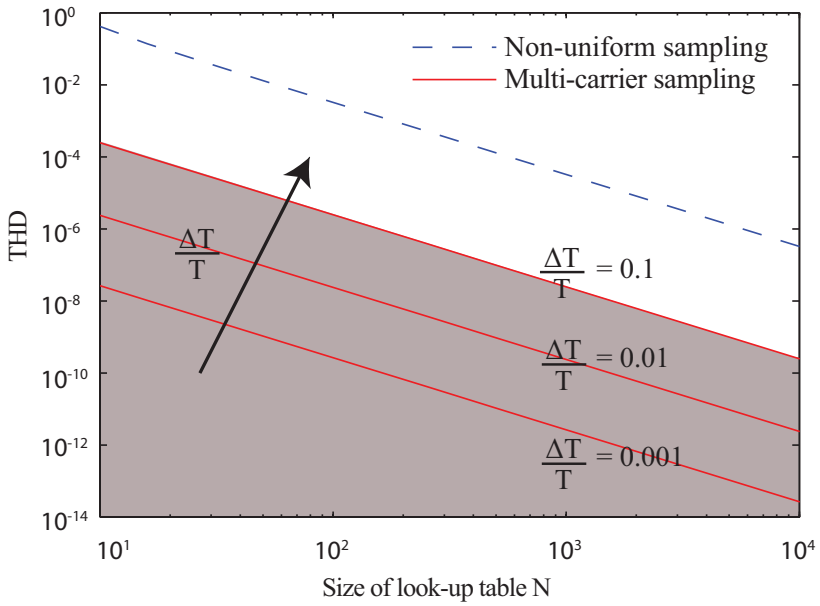

Figure 2.4: Total harmonic distortion of traditional non-uniformly sampled reference generation and multi-carrier reference generation. The THD decreases as the term $\Delta T/T$ decreases.

2.3 Summary

This chapter established the methodology for a multi-carrier sinusoidal synthesis technique for the digital generation of a reference waveform. The multi-carrier method employs two carrier frequencies that are varied to minimize the cumulative tracking error throughout one output period. The derivation shows that for equivalently sized look-up tables, multi-carrier PWM outperforms non-uniform sampling by greater than one order of magnitude. This method also eliminates all subharmonic components, which are a concern in applications including PV-connected inverters and ac-drives. Implementation details and simulation results are presented in the next chapter.

Chapter 3

Implementation of Multi-Carrier PWM for Inverter Applications

3.1 Period Resolution of Multi-Carrier Digital Synthesis

This section will determine the period resolution of multi-carrier digital synthesis and compare it to the resolution of uniformly and non-uniformly sampled digital synthesis. In uniform sampling, the look-up table is sampled at an integer rate such that to retrieve the next sample, a pointer is incremented a set amount. Under these circumstances, only one addition and one fetch operation is typically needed (not including the edge case), as well as a set operation for PWM output. No multiplication is needed to generate the unitary sinusoidal reference. While such an approach does not generate any distortion in the generated reference, the discrete set of carrier frequencies may not contain the nominal inverter frequency.

For a digital PWM module, each carrier period T is an integer multiple of a clock-period. Using the notation developed earlier, the clock-period is the minimum difference between two achievable carriers, ΔT. In this case, the set of all achievable periods, S_T can be determined from (1.2) by defining an integer factor p, and assuming uniform sampling $r = 1$. The integer factor p is set through a register in the microprocessor, and is the maximum count for the PWM counter. The set of all achievable periods is presented below.

$$S_T = \{Np\Delta T \mid p, N \in \mathbb{N}\} \tag{3.1}$$

The term ΔT is limited by the PWM clock module, and is directly related to the cost of the microcontroller. The resolution of T_0 can then be defined as:

$$\begin{aligned} \Delta T_0 &= inf\{x - y \mid x, y \in S_T, x \neq y\} \\ &= N\Delta T \end{aligned} \tag{3.2}$$

In grid-synchronization applications, this resolution in general leads to a deviation of the operating inverter frequency from the grid frequency. Minimizing this deviation is an important consideration in applications that require precises frequency synthesis. The multi-carrier method is able to greatly decrease ΔT_0 compared to the uniform-sampling method. For the multi-carrier method, the set of all achievable T_0 is given in (3.3).

$$\begin{aligned} S_T &= \{\lambda T_1 + (N - \lambda) T_2 \mid \lambda, N \in \mathbb{N}, \lambda \leq N\} \\ &= \{(\lambda + Np) \Delta T \mid \lambda, N, p \in \mathbb{N}, \lambda \leq N\} \end{aligned} \tag{3.3}$$

The resolution of T_0 can be defined using a similar argument as before.

$$\begin{aligned} \Delta T_0 &= inf\{x - y \mid x, y \in S_T, x \neq y\} \\ &= \Delta T \end{aligned} \tag{3.4}$$

The results of (3.4) are that the inverter frequency deviation does not grow with N, unlike

in the case of uniformly sampled digital synthesis. This formulation assumes that λ can take any integer value, although as shown in Chapter 2, it is often wise to limit λ to even values only. This limitation will double the quantization ΔT_0 in (3.4). For non-uniformly sampled digital synthesis with $r \in \mathbb{R}$, the maximum frequency deviation is related to the number of bits used to represent r, and can be quite small, but comes with an increase in THD [16].

It is often more helpful to view the frequency quantization, rather than the period quantization. As per the definition above, the PWM output period is composed of λ pulses at carrier frequency $1/T_1 = f_1$ and $N - \lambda$ pulses at carrier frequency $1/T_2 = f_2$. Based on this, the equation for the PWM fundamental frequency can be expressed as follows.

$$f_0 = \frac{f_1 f_2}{f_2 \lambda + (N - \lambda) f_1} \tag{3.5}$$

The minimum change in output frequency can be determined by finding the difference between (3.5) and a frequency generated by incrementing λ. The result is a definition for the frequency resolution capable of using multi-carrier PWM.

$$\Delta f_0 = \left| f_0 \frac{f_2 - f_1}{\frac{f_1 f_2}{f_0} + (f_2 - f_1)} \right| \tag{3.6}$$

It can be shown that $f_2 - f_1 = f_1 f_2 \Delta T$. Using this equation the frequency resolution can be simplified.

$$\Delta f_0 = \frac{f_0^2}{f_{clk} + f_0}$$

$$\approx \frac{f_0^2}{f_{clk}} \tag{3.7}$$

In (3.7), the term $f_{clk} = 1/\Delta T$ is the clock period. This equation enables an insight that

for multi-carrier PWM, the frequency resolution only depends on the fundamental period and the clock period. By performing a similar analysis for uniform sampled PWM, it can be shown that the frequency resolution for uniform sampling is $\Delta f_0 = \frac{f_0}{T f_{clk}}$. The application of these insights leads to an overall quantization reduction of $\frac{T_0}{T} = N$.

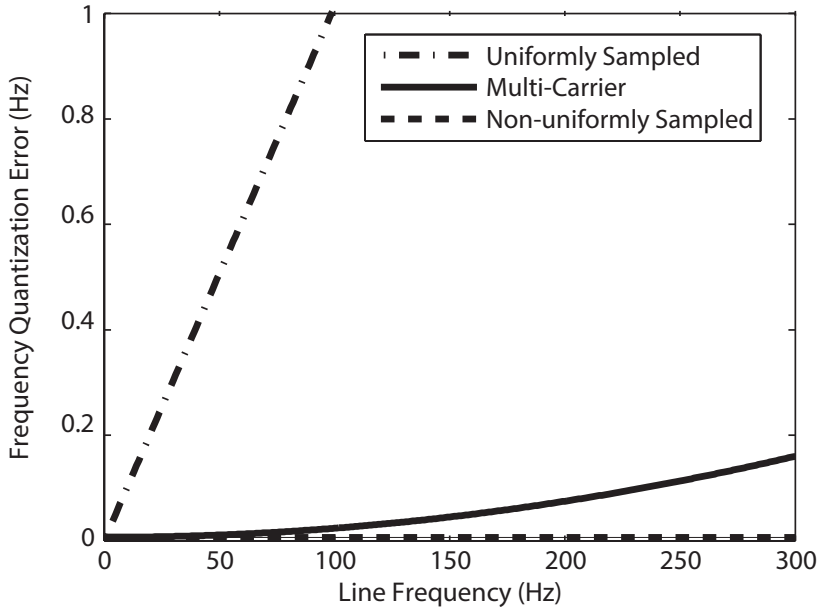

Figure 3.1: Frequency resolution capabilities in uniform, non-uniform, and multi-carrier sinusoidal synthesis, presented for a microcontroller with $f_{clk} = 0.6MHz$, $N = 120$ and variable fundamental frequencies. Uniformly-sampled reference has frequency quantization error that grows with both fundamental and carrier frequency. Multi-carrier frequency error only grows with fundamental frequency, and non-uniform carrier generation has frequency quantization error that grows with carrier frequency.

Fig. 3.1 compares the frequency resolution of multi-carrier sinusoidal synthesis, uniform sampling sinusoidal synthesis, and non-uniform sampling sinusoidal synthesis of a controller with $16 - bit$ registers. To make this comparison, a reference frequency is compared to $N = 120$ carrier pulses at a frequency of $1/T = 60kHz$. The system chosen in this example has a clock frequency of $f_{clk} = 0.6MHz$. It can be seen that at a reference frequency of $f_0 = 60Hz$, uniform sampling sinusoidal synthesis has a large quantization of $0.6Hz$. By using multi-carrier sinusoidal synthesis, the frequency quantization is improved to 0.01.

As mentioned in Chapter 1, the frequency resolution of non-uniform sampling is fixed and dependent only on the register size in the microcontroller.

3.2 Implementation

To implement multi-carrier sine generation in a microcontroller, a table of N equally spaced samples corresponding to $sin(n\frac{2\pi}{N}), n = 0, 1, ..., N-1$ is stored in memory. Each PWM period, a pointer referencing the samples is incremented by a fixed amount and a new sample is fetched. A frequency variation pattern corresponding to the λ/N states available must be stored in memory, but as this pattern is binary in nature, the total memory required is M bits, where M is is the denominator of the reduced fraction λ/N.

For a chosen average carrier period T and number of samples N, the two carriers T_1, T_2 are chosen subject to the following constraints, where p is an integer.

$$\begin{aligned} T_1 =& p\Delta T + \Delta T \\ T_2 =& p\Delta T \\ T_2 \leq& T \leq T_1 \end{aligned} \tag{3.8}$$

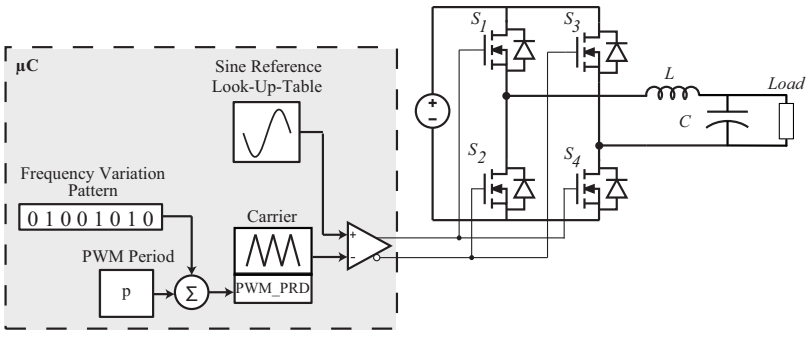

Figure 3.2: A functional diagram of a multi-carrier based single-phase inverter.

Each PWM period, the PWM register PWM_PRD is loaded with $p + d_{\lambda/N}(m)$, where $d_{\lambda/N}(m)$ is the m$^{\text{th}}$ entry in the frequency variation pattern for sequence λ/N and p is given by (3.8). The register PWM_PRD defines the number of clock periods ΔT in one carrier period T. Loading the PWM_PRD in this way enables switching between the two carriers T_1, T_2. A functional diagram of multi-carrier PWM is shown in Fig. 3.2, which describes how the carrier period of the PWM is changed when driving an inverter. As well as the instruction count for fetching the sample, each PWM period requires two additions, two fetch operations, and two set operation. The function $d_{\lambda/N}(m)$ can be defined recursively in terms of (2.15).

$$\begin{aligned} d_{\lambda/N}(m) &= \left\lceil m\frac{\lambda}{N} \right\rceil - d_{\lambda/N}(m-1) \\ d_{\lambda/N}(-1) &= 0 \end{aligned} \tag{3.9}$$

For a sine look-up table of size $N = 16$ implemented in single precision, the look-up table has a size of $64B$. To store the frequency variation sequences for the ratios $\lambda/N = 1/8 \to 7/8$ requires an additional $7B$, much less than is needed to reduce the error by an order of magnitude using the standard method. Each 1 in the frequency variation pattern corresponds to carrier period T_1, as shown in Fig. 3.3. Example $8-$bit frequency variation sequences for multi-carrier sinusoidal synthesis with $N = 16$ is provided in Table 3.1.

Table 3.1: Multi-carrier 8-bit frequency variation patterns.

λ								
2	0	1	0	0	0	0	0	0
4	0	1	0	0	0	1	0	0
6	0	1	0	1	0	0	1	0
8	0	1	0	1	0	1	0	1
10	0	1	1	0	1	1	0	1
12	0	1	1	1	0	1	1	1
14	0	1	1	1	1	1	1	1

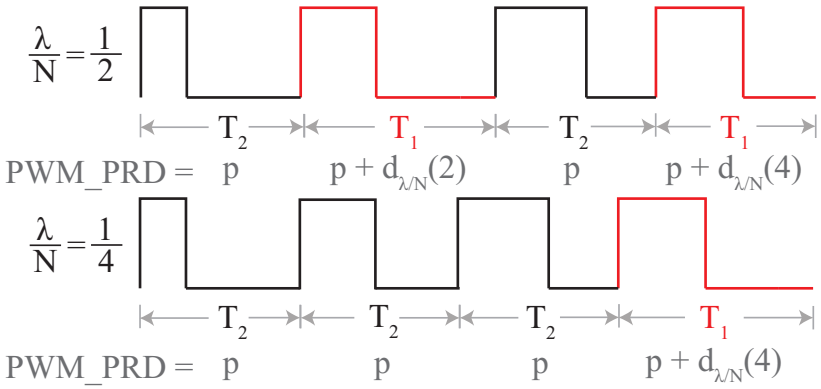

Figure 3.3: Output waveforms of the proposed multi-carrier method. Example multi-carrier patterns of ratio θ/N are used to minimize the THD of the modulated sine wave.

To determine which λ is needed for a given output frequency, simply rearrange (3.3). The result (3.10) provides a simple way of determining which frequency variation pattern to use for optimum reference generation.

$$\lambda = \frac{T_0}{\Delta T} - N \left\lfloor \frac{T_0/\Delta T}{N} \right\rfloor \tag{3.10}$$

Since only integer values of λ can be implemented, it is assumed that $T_0/\Delta T$ is an integer, which allows (3.10) to be written as (3.11). This quantization is caused by the frequency resolution defined in (3.4).

$$\lambda = \left\langle round\left(\frac{T_0}{\Delta T}\right)\right\rangle_N \tag{3.11}$$

Using the equations developed here, a simple yet extremely efficient PWM based sinusoidal synthesis platform can be developed. It is important to note that (3.11) is very susceptible to round-off error, and care should be taken to perform computations with adequate precision. This platform allows for superior performance with modest memory requirements and very low computational burden.

The multi-carrier PWM algorithm is visualized in Fig. 3.4. The algorithm is entered at

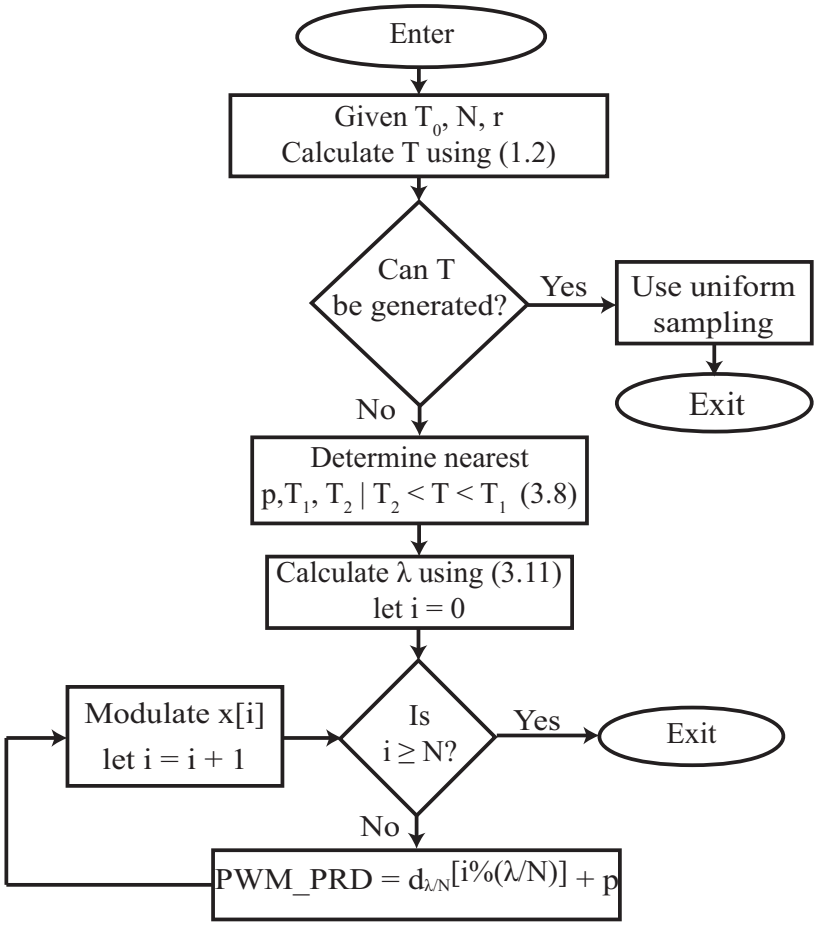

Figure 3.4: Multi-carrier PWM algorithm. After the fundamental period is determined, this algorithm is used to switch between two carriers to synthesize the reference frequency.

the beginning of every output period, and the only information required before entering the multi-carrier PWM algorithm is the desired fundamental output frequency and look-up table size. In the case of an inverter, the fundamental frequency is the driving frequency or the grid-connect frequency. In the case of active rectification of a sinusoidal signal, it is double the input frequency, which can be determined using zero-cross detection. If the fundamental PWM output frequency is attainable using the uniform sampling method (i.e. by outputting an integer N pulses per period at an obtainable carrier frequency) then the carrier frequency can be set by traditional means and the algorithm is exited. When this is not the case, λ needs to be calculated according to (3.11). Using this algorithm, multi-carrier sinusoidal

synthesis can be implemented in a microcontroller or DSP efficiently.

3.3 Simulation

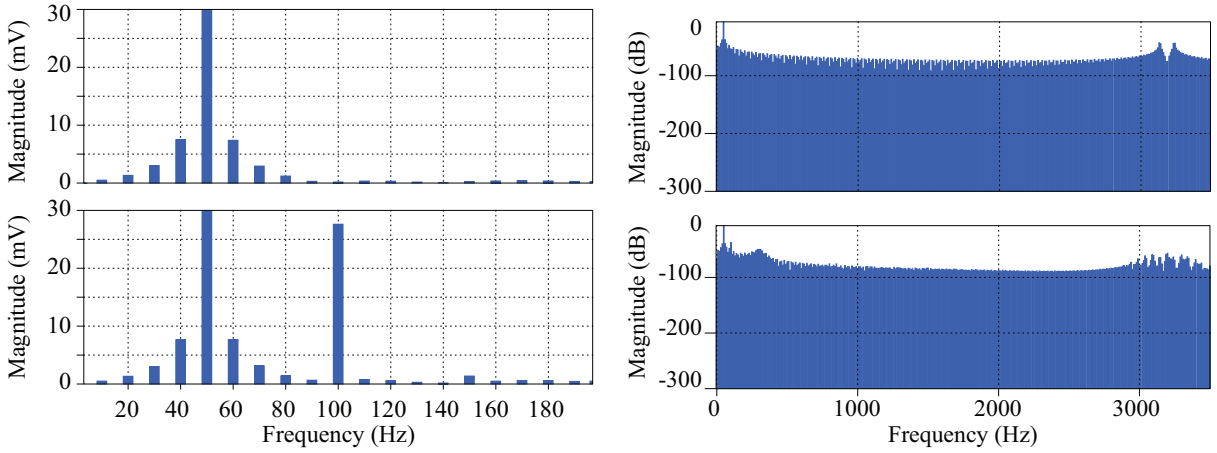

Figure 3.5: Simulation results for a look-up table generated reference (top) and inverter capacitor voltage (bottom) for a reference generated with a look-up table of size $N = 64$ and non-uniform sampling with $r = 1.0016$. (a) Results presented in mV, relative to the fundamental harmonic to show relative strength of subharmonic distortion (b) Entire spectrum presented in dB, relative to the fundamental harmonic.

To verify the theory presented in this thesis, a simulation was conducted using the PLECS simulation software. A full-bridge inverter was driven with a switching frequency of $3.19kHz$. The inverter had an $100V$ input voltage and an LC filter with values $5.5mH$ and $50\mu F$, giving a cut-off frequency of $304Hz$. A $64-$point look-up table was implemented, with an index multiplier $r = 1.0016$ to ensure a $50.0Hz$ output was generated. The amplitudes of both the reference and harmonic spectrum were scaled such that their peak amplitudes were $1V$, after which the harmonic spectrum of both waveforms were analyzed. These results, presented in Fig. 3.5(a), show that the generated reference exhibits significant sub-harmonic distortion, which remains after the modulation and filtering. Running the simulation again, but with a table size of $N = 1024$ show that sub-harmonic distortion remains, but is reduced such that

it is a minor contributor to the total harmonic spectrum, as seen Fig. 3.6(a). All simulations used $10Hz$ frequency divisions to represent harmonic spectrum including sub-harmonic and overtone effects.

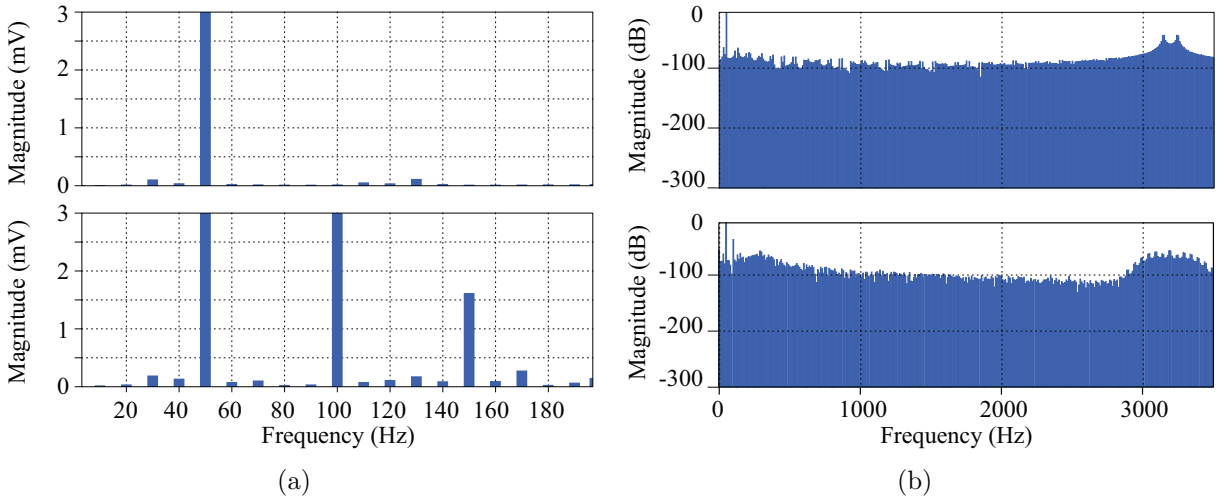

(a) (b)

Figure 3.6: Simulation results for a look-up table generated reference (top) and inverter capacitor voltage (bottom) for a reference generated with a look-up table of size $N = 1024$ and non-uniform sampling with $r = 16.0256$. (a) Results presented in mV, relative to the fundamental harmonic to show relative strength of subharmonic distortion (b) Entire spectrum presented in dB, relative to the fundamental harmonic.

Next, the proposed multi-carrier method was implemented by switching between two carrier frequencies $1/T_1 = 3.19kHz$ and $1/T_2 = 3.21kHz$. The frequency variation ratio is determined through (3.11) to be $\lambda/N = 32/64$, and is chosen to ensure an output frequency of $1/T = 50.0Hz$. The results, presented in Fig. 3.7(a), show that the generated reference exhibits no sub-harmonic distortion.

Using the simulation data, the THD was calculated and presented in Table 3.2. It can be seen that for the reference signal, the multi-carrier sinusoid has a much lower THD than do non-uniform sinusoidal synthesis, as predicted in Fig.2.4. This difference is largely mitigated by increasing the table size to $N = 1024$ for non-uniformly sampled sinusoidal generation. When comparing the THD of the inverter's capacitor voltage, it can be seen that this reference-induced harmonic distortion leads to a 2% change, and does so without increasing

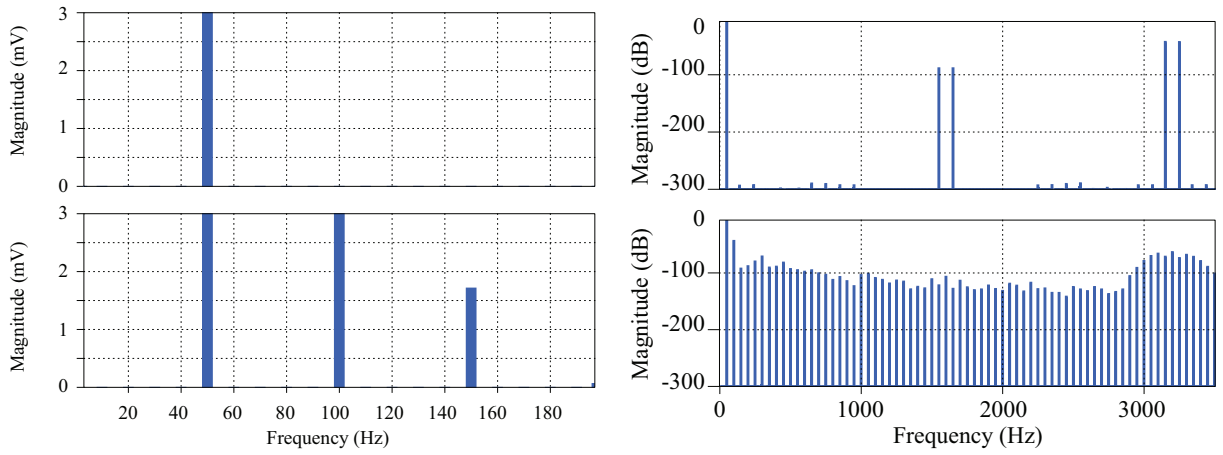

(a) (b)

Figure 3.7: Simulation results for a look-up table generated reference (top) and inverter capacitor voltage (bottom). A multi-carrier look-up table of size $N = 64$ with $\lambda/N = 32/64$. (a) Results presented in mV, relative to the fundamental harmonic to show relative strength of subharmonic distortion (b) Entire spectrum presented in dB, relative to the fundamental harmonic.

Table 3.2: THD simulation results for sinusoidal generation.

	Reference Waveform	Capacitor Voltage Waveform
Multi-Carrier $N = 64$	7.85×10^{-3} %	2.77%
Non-uniform $N = 64$	3.58%	4.81%
Non-uniform $N = 1024$	1.69×10^{-1} %	2.83%

the number of points N or using computationally expensive interpolation.

3.4 Experimental Results

To verify the multi-carrier PWM technique, the algorithm was tested in a Texas Instruments TMS320F28335 DSP. A $100V$ input voltage was applied to a full-bridge inverter, which is

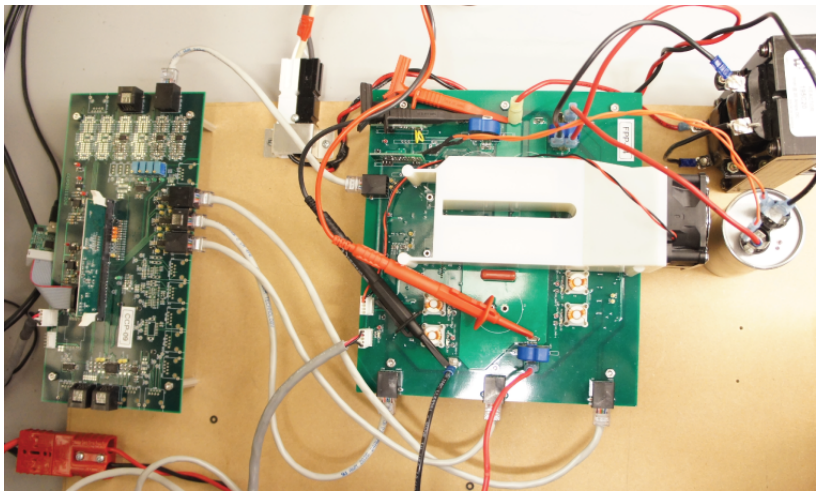

Figure 3.8: The full-bridge inverter prototype used in experiments comprised of the control card (left) and invterter module (right).

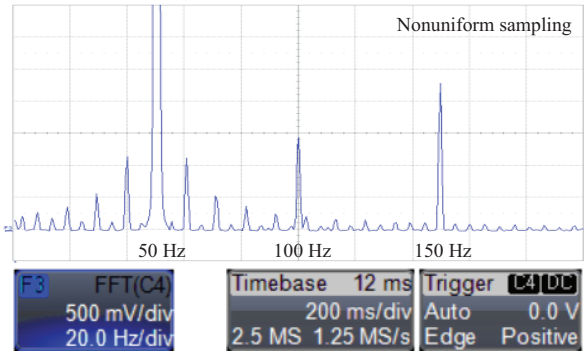

(a)

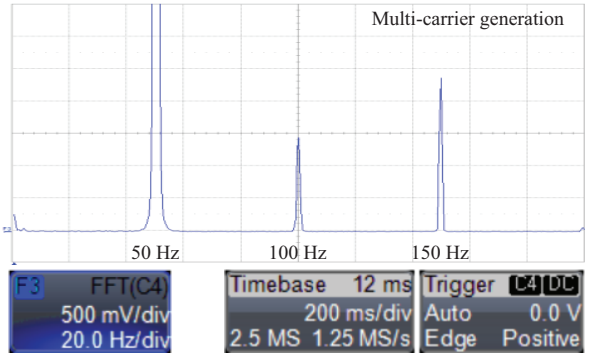

(b)

Figure 3.9: The output spectrum of an inverter implementing a look-up table of size $N = 64$. (a) Non-uniform sampling with $r = 1.0016$ to ensure an output frequency of $50.0Hz$, (b) A multi-carrier look-up table with $\lambda/N = 32/64$ to ensure an output frequency of $50.0Hz$

Table 3.3: Component list and design parameters for inverter prototype.

Component	Part-Number
μC	Texas Inst. TMS320F28335
MOSFET S_1,S_2,S_3,S_4	Micrel Inc. MIC4421ZM TR
C	50 μF
L	3 mH
Design Parameter	**Value**
v_{in}	100 V
T_0	0.02 s
N	64
$1/T_1$	3.19 kHz
$1/T_2$	3.21 kHz
$1/T_{clk}$	1 MHz
m, modulation index	0.9

controlled by the PWM output of the microcontroller. For simplicity, a sawtooth carrier reference is used for the PWM module. The PWM output was filtered through an LC filter to produce the inverter output. The prototype and experimental set-up is shown in Fig. 3.8. Component list and design parameters are listed in Table 3.3. Refer to Fig. 3.2 for a circuit diagram with component labels.

To summarize the algorithms operating point, the experimental conditions are presented as follows. A moderate clock of $1MHz$ is used to generate the DPWM output. A look-up table of size $N = 64$ was uploaded to the memory to generate the sine reference. To minimize switching losses, a low carrier frequency of $1/T = 3.19kHz$ was used. Using a standard implementation, a sampling multiplier of $r = 1.0016$ is necessary to accurately generate the correct output frequency. For multi-carrier PWM, the carrier frequencies $1/T_1 = 3.19kHz$ and $1/T_2 = 3.21kHz$ are used. The calculated frequency variation fraction is $\lambda/N = 31/64$, but to eliminate subharmonic components, this was changed to $\lambda/N = 32/64$.

The output spectrum of the inverter caused by the signals generated through non-uniform sampling and multi-carrier PWM are presented in Fig. 3.9(a) and Fig. 3.9(b), respectively. It can be seen through inspection that there is significantly less distortion for the sinusoidal

output generated with multi-carrier PWM, and no subharmonic distortion is visible.

3.5 Summary

This chapter established the methodology for implementing multi-carrier sinusoidal synthesis in low-cost microcontrollers, and by doing so greatly increases the frequency resolution of carrier-based ac-dc/dc-ac power converters for practical applications. Limitations of period resolution are developed and linked to the distortion existing in the digital reference generation. Simulation results verify that this distortion produces an increased THD in voltage controlled inverters. Experimental results were conducted, and the elimination of sub-harmonic components verified. This chapter provides a simple, computationally inexpensive method for decreasing the THD in inverters and other sinusoidal synthesis applications without increasing the memory requirements nor the cost of the micro-controller.

Chapter 4

Ripple Elimination In Closed-Loop Digital Converters

4.1 Analysis of a Moving Average Filter

Traditionally, single-phase power factor correctors suffer from a slow response time, characterized by a low voltage loop bandwidth ($< 1Hz$) that is necessary to ensure a suitable THD in the input current. This chapter examines the use of practical discrete filters to substantially improve the voltage feedback-loop bandwidth. As a result of the following analysis, the moving averaging filter (MAF) proves to be an effective solution. The analysis shows that it is an excellent practical filter for PFC control, and requires low computational overhead and basic discrete signal theory literacy for its implementation.

A moving average filter is defined as the average of the current input with M past samples, where M is defined as the kernel size. Mathematically, the impulse response of a MAF is defined as:

$$h[n] = \frac{1}{M+1} \sum_{k=0}^{M} \delta[n-k] \tag{4.1}$$

where $\delta[n-k]$ is an impulse delayed by k samples. By transforming (4.1) using a discrete Fourier transform (DFT) the frequency response is determined [41].

$$H(e^{j\omega}) = \frac{1}{M+1}\sum_{n=0}^{M} e^{-j\omega n} \tag{4.2}$$

Using the closed-form of the general geometric series, the frequency response is simplified.

$$H(e^{j\omega}) = \frac{1}{M+1}\frac{1-e^{-j\omega(M+1)}}{1-e^{-j\omega}} \tag{4.3}$$

Lastly, after some simple rearrangement, an analytically descriptive representation is developed.

$$H(e^{j\omega}) = \frac{1}{M+1}\left[\frac{sin(\omega(M+1)/2)}{sin(\omega/2)}\right]e^{-j\omega M/2} \tag{4.4}$$

By analyzing (4.4), insights into the operation and effect of a MAF can be gleaned. From the amplitude, it can be seen that a number of evenly spaced frequencies are eliminated. From the phase, it is evident that those notched frequencies correspond to a phase jump of 180^o. This phase jump can be interpreted in two ways. First, the frequency components at the notching frequencies experience an infinite time delay. In other words, the notching frequencies are completely removed from the system response. Secondly, the phase jump of 180^o signifies a point of marginal stability. Frequencies approaching the phase jump of 180^o also approach the phase-margin of the system. Components at frequencies near the notching frequencies may experience instabilities, and should therefore be attenuated. For the comb and notch filter, this instability region can be minimized by increasing r coefficient, but this can increase the cost and complexity of the filter in fixed-point systems.

The implementation a MAF filter in the finite impulse response (FIR) form given in (4.5) has an algorithmic asymptotic complexity of $\Omega(M)$, which is not suitable for a real-time implementation. Instead, an infinite impulse response (IIR) form is needed to reduce the computational burden. The FIR form of the filter is presented below.

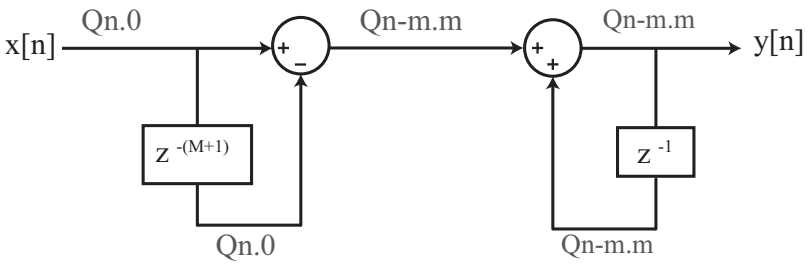

Figure 4.1: The signal diagram of a MAF filter in a fixed-point microprocessor showing Q-notation and implicit division.

$$y[n] = \frac{1}{M+1} \sum_{k=0}^{M} x[n-k] \tag{4.5}$$

To determine the IIR, the following derivation is presented. The first term can be taken out of the summation and an $M+1$ term can be added to the summation as follows.

$$y[n] = \frac{1}{M+1} \left(\sum_{k=1}^{M+1} x[n-k] + x[n] - x[n-(M+1)] \right) \tag{4.6}$$

Next, the summation limits are adjusted by decrementing the index.

$$y[n] = \frac{1}{M+1} \left(\sum_{k=0}^{M} x[(n-1)-k] + x[n] - x[n-(M+1)] \right) \tag{4.7}$$

Lastly, the summation term is recognized to be the previous output term $y[n-1]$.

$$y[n] = \frac{x[n] - x[n-(M+1)]}{M+1} + y[n-1] \tag{4.8}$$

The real advantage of the MAF filter is its simple implementation, even in fixed-point microprocessors, as shown in Fig. 4.1, which shows the signal diagram of the algorithm and the Q-notation representation of fixed-point signal. Notice that if $M+1$ is chosen to be a power of 2, then the division is achieved by an implicit shift of the radix point. For instance, assume $M+1 = 64$, therefore $m = log_2 64 = 6$bits. The input value is already a fixed-point

integer represented by, for example, $n = 8$bits. Therefore, the input signal is in form $Q8.0$. Q-notation is the standard approach to describing fixed-point integer representation where two integers represent the number of bits before and after the radix point, in this case 8 and 0 respectively. After the input delay, instead of dividing the value by 64 (and losing 6-bits of accuracy), the signal is assumed to be of form $Q2.6$. This is an implicit change in representation and does not affect how the data is stored, nor does it introduce any loss of accuracy.

Because there are no coefficients in the MAF-filter, no rounding error is introduced [42]. This rounding error can be detrimental to digital filter's performance and stability, and can greatly influence the size of the registers associated with the algorithm [43]. Unlike the comb and notch filters, the MAF filter is not affected by the coefficients' accuracy due to register sizing. Instead, the register size is only restricted by the number of bits necessary to avoid overflow during reasonable operating conditions. The simplicity of the filter therefore leads to a potentially cheaper and simpler implementation.

For a MAF filter, the first notch of which is set to a specific frequency f_0, it can be shown that for moderate to large sized kernels, the response time is approximately the same. To perform this analysis, we will need to define the concept of group delay. Group delay is defined as the digital delay, measured in number of samples, that each frequency component of an input passed through a digital filter will experience [41]. At points where the phase response of the MAF filter is differentiable (i.e. everywhere besides notching frequencies), the group delay is defined as follows.

$$t_g = \frac{M}{2} \tag{4.9}$$

Equation (4.9) shows that, neglecting the notching frequencies, a MAF filter causes a constant group delay of $M/2$. To convert the group delay to a time delay, the sample time

must be taken into account. The time delay caused by a MAF can be written as follows, where f_s is the sample frequency of the MAF.

$$t_d = \frac{M}{2f_s} \tag{4.10}$$

The sample frequency and kernel size are constrained by the following equation, where f_0 is the frequency of the first notch.

$$f_s = (M+1)f_0 \tag{4.11}$$

Substituting this constraint into (4.10), the delay is determined in terms of the kernel size and the primary notching frequency.

$$t_d = \frac{M}{2f_0(M+1)} \tag{4.12}$$

Minimizing (4.12), it can be seen that the fastest response is for smaller kernel sizes, M, but this can cause higher distortion in the inductor current during transients due to the small sample rates. As M is increased, the delay quickly approaches the maximum time delay $t_d = \frac{1}{2f_0}$. This means that for large kernels, the theoretically shortest recovery time from a step-change in the load is half the line period. This delay is larger than that seen in the comb and notch filter (of appropriately chosen r-values) and leads to a larger voltage drop during step-transients. Fortunately, the linear phase makes it simple to compensate for the time delay.

Since the response time quickly approaches the maximum delay for large M, the sizing of the kernel should be chosen independently of the response time. The sample time f_s should be chosen such that the kernel size $f_s/f_0 = M+1$ is a power of 2 in order to enable simple fixed-point division. Increasing M raises cost by requiring larger registers to perform the

algorithm without introducing truncation error.

4.2 Simulation and Experimental Results

The PFC was simulated with and without a MAF in the voltage feedback loop, as presented in Fig. 4.2(a) and Fig. 4.2(b). The voltage and current loops are controlled with digital PI controllers. In the simulation, a PFC is implemented with a reference output voltage of $V_r = 300V$, input voltage of $V_i = 120V_{rms}$, circuit parameters of $L = 800\mu H$ ad $C = 660\mu F$, and a switching frequency of $f_s = 60kHz$. To analyze transient behavior, the system is loaded with a current step-up.

Without filtering, the PI controller was calibrated to cause little overshoot while maintaining a THD of 3%. At $t = 500ms$ the load changes from a 1A to 2A load. This causes a 5% drop in voltage and the system does not recover for $t = 100ms$, where recovery is judged as a mean deviation of 1% from the reference voltage. Next, a MAF was placed in the voltage feedback loop of the PFC. Again, a PI controller was calibrated to cause little overshoot. The PFC was simulated with the same conditions as before, but resulted in a THD of 1% due to the MAF. The increased bandwidth resulted in an 3% drop in the bus and the system recovered in $t = 25ms$.

To verify the MAF performance in single-phase PFCs, the algorithm was tested in a Texas Instruments TMS320F28335 DSP. A $120V_{rms}$ sinusoidal input voltage was applied to a rectifier and a boost-converter was controlled to emulate a constant resistance. The prototype and experimental set-up is shown in Fig. 4.3. Design parameters are listed in Table 4.1. Refer to Fig. 1.3 for a circuit diagram with component labels. Simulation results are verified experimentally under the same operating conditions and are presented in Fig. 4.4(a) and Fig. 4.4(b). The PI compensator is chosen such that the inductor current THD is 5% in both figures. Voltage drop and recovery time is significantly improved by the inclusion of a MAF

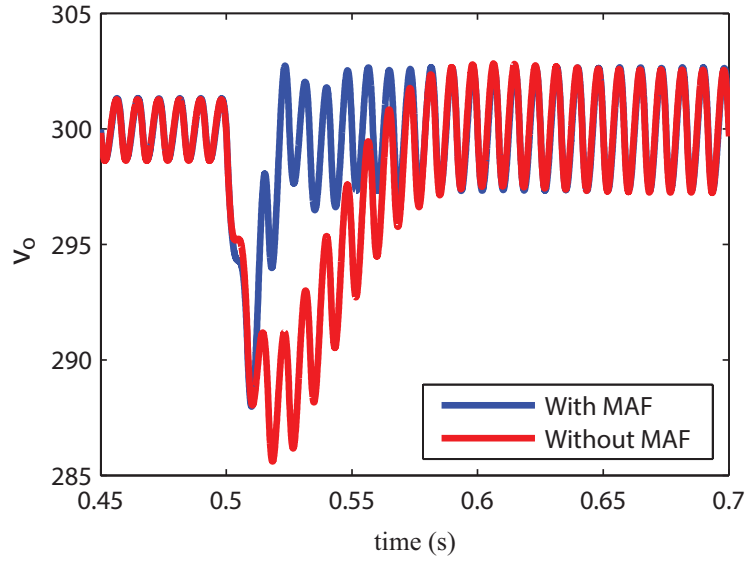

(a)

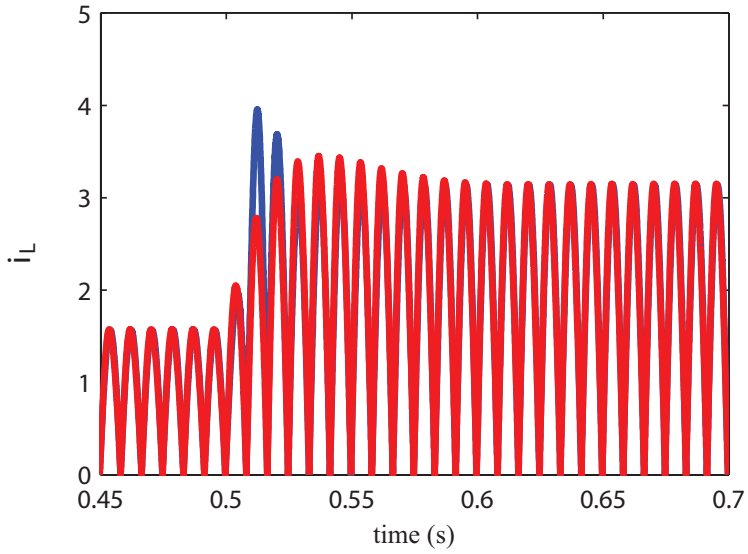

(b)

Figure 4.2: Simulation results for a PI compensated PFC with and without a MAF filter. (a) The capacitor voltage transient after a current load step-up. (b) The inductor current transient current load step-up.

in the voltage control loop, which coincides with the simulation results.

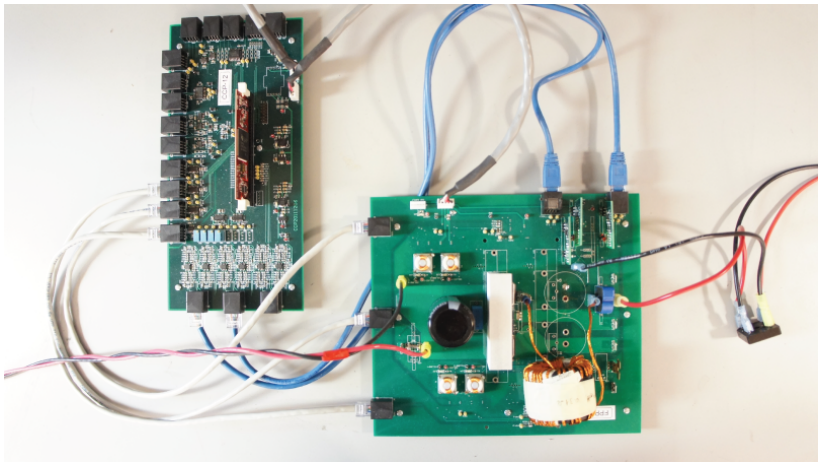

Figure 4.3: The single phase PFC prototype used in experiments comprised of the control card (left) and PFC (right).

Table 4.1: Component list and design parameters for PFC.

Component	Part-Number
μC	Texas Inst. TMS320F28335
Rectifier	Vishay GBPC2506
MOSFET S	Int. Rectifier IRFP460A
Diode D	Fairchild Semi. RHRP1560
C	560 μF
L	577 μH
Design Parameter	**Value**
v_i	120 V_{rms}
v_o	300 V
f_s	60 kHz
MAF kernel $M+1$	64
i_L THD	5%

4.3 Filter Comparison

The results show that by incorporating a MAF in the feedback loop, the performance of a PFC can be greatly increased. Fig. 4.5 compares the MAF with the digital notch and comb filter, for a roll-off factor of $r = 0.9$. The roll-off factor r determines how quickly the filter attenuates near the filter frequency. A noticeable difference in these filters are the dc gains. The MAF provides a unitary gain for the dc component, whereas the comb and notch filters

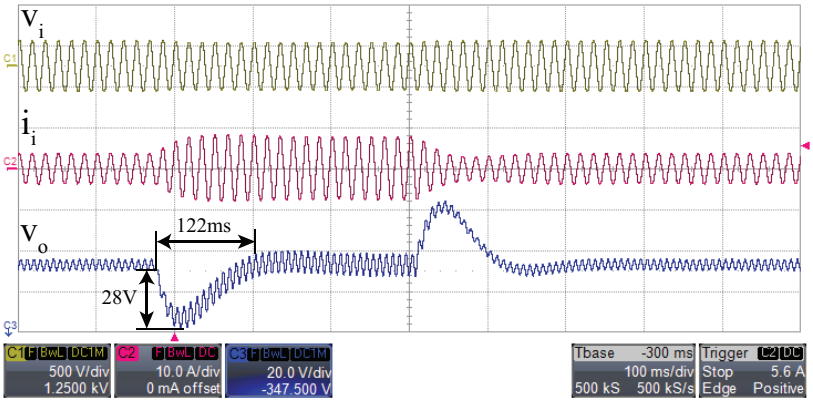

(a)

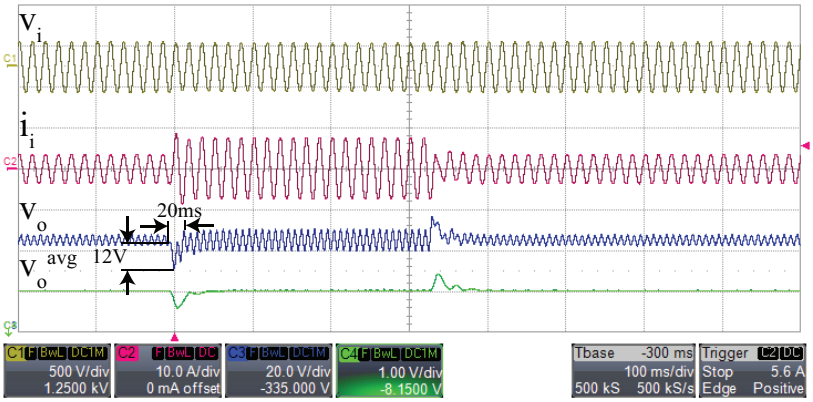

(b)

Figure 4.4: Experimental results for a PI compensated PFC for current step: (a) Without a MAF filter, (b) With a MAF filter of kernel size $M + 1 = 64$. For both captures: input voltage (Ch1), input current (Ch2), output voltage (Ch3). For (b) only: MAF-averaged output voltage (Ch4).

will need additional gain adjustment to avoid a steady state error in the voltage control loop. Fig. 4.5 show that all three filters reach the 180^o phase shift at the same frequency, the notching frequency, giving each filter the same instability points. The larger slope, and greater group-delay in the MAF, corresponds to a larger voltage-drop and potentially larger marginal-stability region than is present in the notch and comb filter. This is balanced by the lack of coefficients and the resultant decrease in computation and memory requirements, effectively reducing the cost of the micro-controller. The micro-controller requirements are summarized in Table 4.2, where computational burden is defined as the number of operations

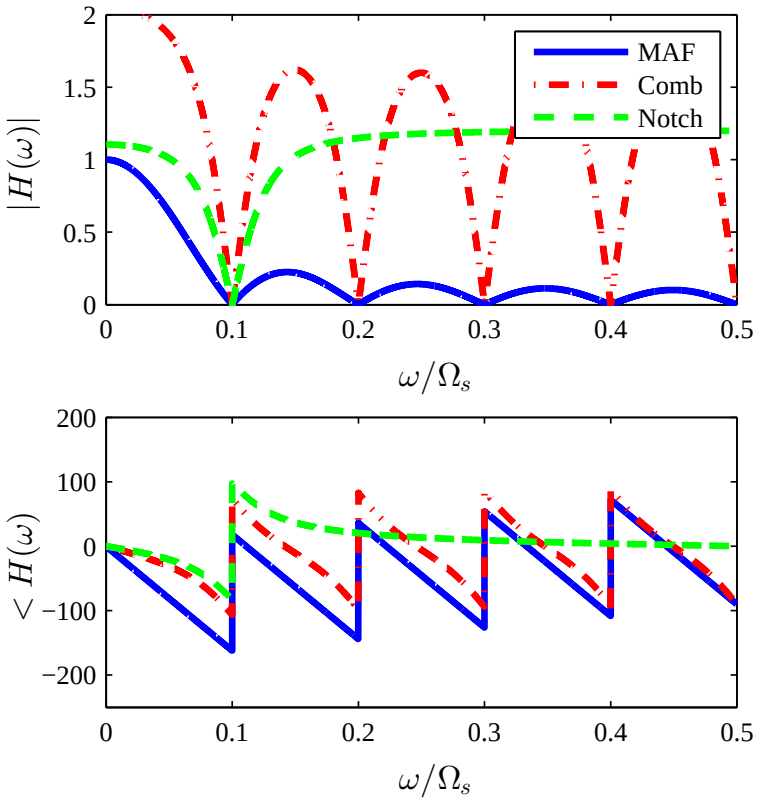

Figure 4.5: Amplitude and phase response comparison of a MAF, Comb and digital notch filter with a roll-off factor of $r = 0.825$. (b)The signal diagram of a MAF filter showing Q-notation and implicit division.

Table 4.2: Comparison of digital filter techniques.

	Memory (values)	Comp. Burden	Ripple Eliminated
No Filter	0	None	No
Notch	4	8 OPC	Partial
MAF	M	2 OPC	Yes
Comb	2M+2	11 OPC	Yes

per cycle (OPC).

4.4 Summary

Through comparative analysis, a moving average filter was presented as a means to increase the dynamic response of a typical PFC while simultaneously reducing the THD of the inductor current. The MAF was shown to significantly increase performance compared to traditional low-pass-filtering techniques, resulting in a PFC capable of recovering from a load-step increase in half the time obtainable traditionally. The dynamics of the MAF filter were compared to previously proposed digital filters, such as the digital notch and comb filter. The MAF presents results comparable to the comb filter, requiring half the memory and minimal computational burden, providing an efficient and effective solution for practical implementation.

Chapter 5

Conclusion

5.1 Summary

This thesis introduced the multi-carrier PWM technique for digital sinusoidal synthesis. This method is introduced as an alternative to non-uniformly sampled sinusoidal synthesis, which exhibits sub-harmonic distortion and large THD, and uniformly-sampled sinusoidal synthesis, the frequency resolution of which can be unsuitable for many applications. Multi-carrier PWM has been shown to be a computationally inexpensive technique, requiring no specialized hardware, unlike previously proposed interpolation techniques.

The multi-carrier technique was studied in relation to the single-phase voltage-controlled inverter. It was shown to generate an accurate reference with significantly less memory than do non-uniformly sampled sinusoidal synthesis, and simulations verified that this leads to a decrease in THD by 2%. Through experimental verification, it was also shown that no sub-harmonic distortion is present in the inverter output. The fundamental period resolution is dependent on the clock-frequency of the micro-controller, and is independent of the number of samples per period.

The second discrete signal processing contribution presented in this thesis was the application of moving average filter to the single-phase PFC voltage feedback loop. The MAF was analyzed and compared to existing digital filtering techniques for single-phase power factor correctors. The simple implementation of MAF, along-with computational simplicity, makes MAF a great filter for practical PFC design in low-margin industries. Through experiments

and simulation, it was shown that through the use of MAF, PFCs respond to load-changes in approximately half the time that traditional PI controllers do, while maintaining or reducing THD.

The work presented in this thesis was published at IEEE APEC 2013 [2] and IEEE ECCE 2013 [3], and submitted for publication [1].

5.2 Future Work

The original contributions in this thesis in the field of multi-carrier sinusoidal synthesis only consider the case of two distinct carrier frequencies. By expanding this technique to include an arbitrary number of distinct carrier frequencies, a new method of generating periodic signals can be devised that require a minimum number of stored elements. By including an infinite number of carrier frequencies, with an infinitesimally small resolution, this can also lead to a method which better analyzes variable-frequency controllers such as hysteresis or bang-bang PWM controllers. Lastly, this technique can be expanded for use in other applications where high precision periodic signal generation is necessary.

The application of MAF for the simple, efficient filtering of harmonics can be extended to various applications with swinging buses, such as fuel-cell power conversion and solar power conversion. These platforms will exhibit a dc-output with a $120Hz$ pulsating ripple, the filtering of which will enable a much higher bandwidth without increasing the distortion.

Bibliography

[1] J. Forbes and M. Ordonez, "Improved Digital PWM using Multi-Carrier Digital Sine Generation for Inverters," submitted to IEEE Transactions in Industrial Electronics, Aug. 2013

[2] ©2013 IEEE. Reprinted, with permission, from J. Forbes, M. Ordonez, and M. Anun, "Increased Frequency Resolution of Active Rectifiers Using Fractional Digital PWM", IEEE Applied Power Electronics Conference and Exposition," Long Beach (California), March 2013

[3] ©2013 IEEE. Reprinted, with permission, from J. Forbes, M. Ordonez, and M. Anun, "Improving the Dynamic Response of Power Factor Correctors Using Simple Digital Filters: Moving Average Filter Comparative Evaluation," IEEE Energy Conversion Congress and Exposition, Denver (Colorado), Sept. 2013

[4] J. Tierney, C. M. Rader, and B. Gold, "A Digital Frequency Synthesizer," IEEE Transactions on Audio and Electroacoustics, vol.AU-19, no.1, pp. 48-57, Mar. 1971

[5] S. Mehrgardt, "Noise Spectra of Digital Sine-Generators Using the Table-Lookup Method," IEEE Transactions on Acoustics, Speech, and Signal Processing, vol.ASSP-31, no.4, pp. 1037-1039, Aug. 1983

[6] D. A. Grant, M. Stevens, and J. A. Houldsworth, "The effect of Word Length on the Harmonic Content of Microprocessor-Based PWM Waveform Generators," IEEE Transactions on Industry Applications, vol.IA-21, no.1, pp. 218-225, Jan. 1985

[7] B. Diong, H. Sepahvand, and K. A. Corzine, "Harmonic Distortion of Cascaded H-Bridge Inverters Considering Device Voltage Drops and Noninteger DC Voltage Ratios," IEEE Transactions on Industrial Electronics, vol.60, no.8, pp. 3106-3114, Aug. 2013

[8] F. Filho, H. Zandonadi, T. H. A. Mateus, B. Ozpineci, L.N. Tolbert, and J. O. P. Pinto, "Adaptive Selective Harmonic Minimization Based on ANNs for Cascade Multilevel Inverters with Verying DC Sources," IEEE Transactions on Industrial Electronics, vol.60, no.5, pp. 1955-1962, May 2013

[9] R.W. Erickson and D. Maksimovic, "Fundamentals of Power Electronics," 2nd ed. Norwell, Mass. : Kluwer Academic, 2001.

[10] R. Ridley, "Power Supply Design Volume 1: Control," 1st ed. Monpazier, France : Ridley Engineering, 2012.

[11] Y. Zhang, W. Xu, Y. Yu, "The PFC with Average Current-Mode and Voltage Fuzzy Controller for the Output Voltage," Second International Symposium on Intelligent Information Technology Application, vol.1, pp.771-775, 20-22 Dec. 2008

[12] V.M. Rao, A.K. Jain, K.K. Reddy, A. Behal, "Experimental Comparison of Digital Implementations of Single-Phase PFC Controllers," IEEE Transactions on Industrial Electronics, vol.55, no.1, pp.67-78, Jan. 2008

[13] D.G. Holmes and T.A. Lipo, "Pulse Width Modulation For Power Converters," Piscataway, New Jersey : IEEE Series on Power Electronics, 2003

[14] Y. C. Jenq, "Digital Spectra of non-uniformly Sampled Signals: Fundamentals and High-Speed Waveform Digitizer," IEEE Transactions on Instrumentation and Measurement, vol.37, no.2, pp. 245-251, Jun. 1998

[15] Y. C. Jenq, "Digital Spectra of non-uniformly Sampled Signals: Digital Look-Up Tunable Sinusoidal Oscillators," IEEE Transactions on Instrumentation and Measurement, vol.37, no.3, pp. 358-362, Spet. 1998

[16] T. Abeyasekera, C.M. Johnson, D. J. Atkinson, and M. Armstrong, "Elimination of Subharmonics in Direct Look-Up Table (DLT) Sine Wave Reference Generators for Low-Cost Mictroprocessor-Controlled Inverters," IEEE Transactions on Power Electronics, vol.18, no.6, pp. 1315-1321, Nov. 2003

[17] J. Vankka, "Methods of Mapping from Phase to Sine Amplitude in Direct Digital Synthesis," Proceedings of the 1996 IEEE International Frequency Control Symposium, IEEE Transactions on Power Electronics, pp.942-950, Jun 1996

[18] Texas Instruments, "C28x IQmath Library A virtual Floating Point Engine: Module User's Guide v1.5c," http://www.ti.com/lit/sw/sprc990/sprc990.pdf, pp. 56-59, Jun. 2010

[19] Y. Chen and Y.A. Chau, "A Direct Digital Frequency Synthesizer Based on a New Form of Polynomial Approximation," IEEE Transactions on Consumer Electronics, vol.56, no.2, pp. 436-440, May 2010

[20] A. Ashrafi, R. Adhami, and A. Milenkovic, "A Direct Digital Frequency Synthesizer Based on Quasi-Linear Interpolation Method," IEEE Transactions on Circuits and Systems-I: Regular Papers, vol.57, no.4, pp. 863-871, Apr. 2013

[21] S. R. Bowes, "New Sinusoidal Pulsewidth-Modulated Inverter," Proc. IEE, vol.122, no.11, pp. 1279-1285, Nov. 1975

[22] S. R. Bowes and B. M. Bird, "Novel Approach to the Analysis and Synthesis of Mod-

ulation Processes in Power Converters," Proc. IEE, vol.122, no.5, pp. 507-513, May 1975

[23] P.F. Ksiazek, M. Ordonez, "Swinging Bus Technique for Ripple Current Elimination in Fuel Cell Power Conversion," IEEE Transactions on Power Electronics, vol.29, no.1, pp.170-178, Jan. 2014

[24] J. Holtz, "Pulsewidth Modulation - A Survey," IEEE Transactions on Industry Electronics, vol.39, no.5, pp. 410-420, Dec. 1992

[25] A. Kulkarni and V. John, "Mitigation of Lower Order Harmonics in a Grid-Connected Single-Phase PV Inverter," IEEE Transactions on Power Electronics, vol.28, no.1, pp. 5024-5037, Aug. 2013

[26] J. S. S. Prasad and G. Narayanan, "Minimization of Grid Current Distortion in Parallel-Connected Converters Through Carrier Interleaving," IEEE Transactions on Industrial Electronics, vol.61, no.1, pp. 76-91, Jan. 2014

[27] J. Chavarra, D. Biel, F. Guinjoan, C. Meza, and J. J. Negroni, "Energy-Balance Control of PV Cascaded Multilevel Grid-Connected Inverters Under Level-Shifted and Phase-Shifted PWM," IEEE Transactions on Industrial Electronics, vol.60, no.1, pp. 98-111, Jan. 2013

[28] N. Bodo, E. Levi, and M. Jones, "Investigation of Carrier-Based PWM Techniques for a Five-Phase Open-End Winding Drive Topology," IEEE Transactions on Industrial Electronics, vol.60, no.5, pp. 2054-2065, May. 2013

[29] O. Lopez, D. Dujic, M. Jones, F. D. Freijedo, J. Doval-Gandoy, and Em. Levi, "Multi-dimensional Two-Level Multiphase Spave Vector PWM Algorithm and Its Comparison

With Multifrequency Space Vector PWM Method," IEEE Transactions on Industrial Electronics, vol.58, no.2, pp. 465-475, Feb 2011

[30] S. A. Saleh, C. R. Moloney, and M. A. Rahman, "Analysis and Development of Wavelet Modulation for Three-Phase Voltage-Source Inverters," IEEE Transactions on Industrial Electronics, vol.58, no.8, pp. 3330-3348, Aug. 2011

[31] S. A. Saleh and M. A. Rahman, "Experimental Performances of the Single-Phase Wavelet-Modulated Inverter," IEEE Transactions on Power Electronics, vol.26, no.9, pp. 2650-2661, Sep. 2011

[32] G. Spiazzi, P. Mattavelli, L. Rossetto, "Power Factor Preregulators With Improved Dynamic Response," IEEE Transactions on Power Electronics, vol.12, no.2, pp.343-349, Mar 1997

[33] S. Buso, L. Malesani, P. Mattavelli, "Comparison of Current Control Techniques for Active Filter Applications," IEEE Transactions on Industrial Electronics, vol.45, no.5, pp.722-729, Oct 1998

[34] S. Bhowmik, A. Van Zyl, R. Spee, J. H. R. Enslin, "Sensorless current control for active rectifiers," IEEE Transactions on Industry Applications, vol.33, no.3, pp.765-773, May/Jun 1997

[35] P. Athalye, D. Maksimovic, R. Erickson, "DSP Implementation of a Single-Cycle Predictive Current Controller in a Boost PFC Rectifier," Twentieth Annual IEEE Applied Power Electronics Conference and Exposition, vol.2, pp.837-842 Vol. 2, 6-10 March 2005

[36] W. Zhang, G. Feng, Y.F. Liu, and B. Wu, "DSP Implementation of Predictive Control Strategy for Power Factor Correction (PFC)," Applied Power Electronics Conference and Exposition, vol.1, pp. 67- 73 Vol.1, 2004

[37] A. Prodic, C. Jingquan, R.W. Erickson, D. Maksimovic, "Digitally Controlled Low-Harmonic Rectifier Having Fast Dynamic Responses," Seventeenth Annual IEEE Applied Power Electronics Conference and Exposition, vol.1, no., pp.476-482 vol.1, 10-14 March 2002

[38] S. Buso, P. Mattavelli, L. Rossetto, G. Spiazzi, "Simple Digital Control Improving Dynamic Performance of Power Factor Preregulators," IEEE Transactions on Power Electronics, vol.13, no.5, pp.814-823, Sep 1998

[39] A. Prodic, C. Jingquan, D. Maksimovic, R.W. Erickson, "Self-Tuning Digitally Controlled Low-Harmonic Rectifier Having Fast Dynamic Response," IEEE Transactions on Power Electronics, vol.18, no.1, pp. 420- 428, Jan 2003

[40] A. Prodic, C. Jingquan, R.W. Erickson, D. Maksimovic, "Self-Tuning Digital Comb Filter for PFC Applications," IEEE 2002 28th Annual Conference of the Industrial Electronics Society, vol.1, pp. 220- 225 vol.1, 5-8 Nov. 2002

[41] A. Oppenheim, R. Schaffer, J. Buck, "Discrete Time Signal Processing," 2nd ed. Upper Saddle River, New Jersey : Prentice Hall, 1998.

[42] J.L. Long and T.N. Trick, "A Note on Absolute Bounds on Quantization Errors in Fixed-Point Implementations of Digital Filters," IEEE Transactions on Circuits and Systems, vol.22, no.6, pp. 567-570, Jun 1975

[43] J. Carletta, R. Veillette, F. Krach, Z. Fang, "Determining Appropriate Precisions for Signals in Fixed-Point IIR Filters," IEEE 2003 Design Automation Conference, pp. 656-661 2-6 Jun. 2003